Applied Thermal Engineering 169 (2020) 114914

Contents lists available at ScienceDirect

Applied Thermal Engineering

journal homepage: www.elsevier.com/locate/apthermeng

Direct solar production of medium temperature hot air for industrial applications in linear concentrating solar collectors using an open Brayton cycle. Viability analysis

Antonio Famiglietti[a,*], Antonio Lecuona-Neumann[a], José Nogueira[b], Mohammad Rahjoo[a]

[a] Universidad Carlos III de Madrid, Departamento de Ingeniería Térmica y de Fluidos, Avda. de la Universidad 30, 28911 Leganés, Madrid, Spain
[b] Universidad de Castilla La Mancha, Campus de Excelencia Internacional en Energía y Medioambiente, Escuela de Ingeniería Industrial y Aeroespacial, Av. Carlos III, s/n, Toledo 45071, Spain

HIGHLIGHTS

- Direct air heating inside linear concentrating solar collectors is feasible with current technologies.
- Heat transfer fluid and heat exchanger can be avoided reducing both cost and complexity of solar installation.
- A turbocharger provides the required pumping work, running a greenhouse gases-free direct solar air heater.
- Hot air up to 400 °C for industrial applications is produced.
- Surplus mechanical energy from the turbocharger is useful for pumping the hot air to the user.

GRAPHICAL ABSTRACT

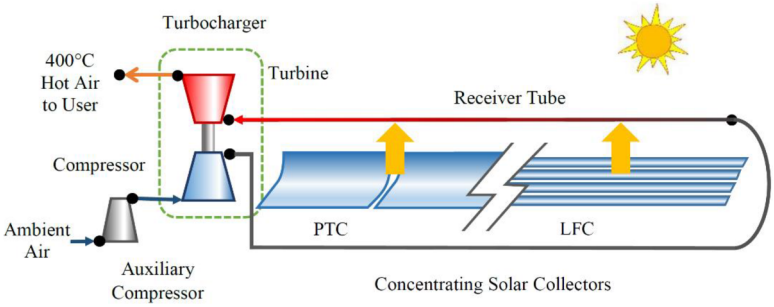

ARTICLE INFO

Keywords:
Solar thermal energy
Direct hot air for industry
Brayton cycle
Linear concentrating solar collectors
SHC
SHIP

ABSTRACT

Medium temperature heat required by industrial processes worldwide is mostly provided consuming fossil fuels. Among renewable energy alternatives, concentrating solar collectors can provide medium temperature heat at decreasing costs, either for medium and small scale applications. Several high energy-demanding processes need hot air in the range 150–400 °C (drying, curing, dehydration, thermal treatments). For such applications, the direct air heating inside linear concentrating solar collectors is investigated in this work. Although is not a common practice, direct heating reduces installation costs and maintenance, eliminating the need for heat transfer fluid and heat exchanger. The theoretical analysis developed indicates its feasibility despite the high pumping power consumption. An innovative system using Brayton cycle is proposed and analyzed. An automotive turbocharger is used to compress inlet air, with a compression ratio from 1.5 to 4, before solar heating up to the technology limit of 600 °C, thus reducing and even avoiding pumping power consumption. Hot air expands through the turbine recovering the compressing power, holding at the outlet suitable temperature for industrial usages in the range of 300–400 °C. No mechanical power at the shaft is expected; instead, turbocharger freewheeling enables to drive air through the collectors without auxiliary energy consumption, configuring a compact solar installation. Numerical results provided support the viability, showing the performances and critical parameters.

* Corresponding author.
E-mail address: antonio_famiglietti@live.it (A. Famiglietti).

https://doi.org/10.1016/j.applthermaleng.2020.114914
Received 10 September 2019; Received in revised form 12 December 2019; Accepted 7 January 2020
Available online 10 January 2020
1359-4311/

Nomenclature

Latin

A	Flow cross-section [m^2]
A_a	Aperture surface area [m^2]
ac	Auxiliary compressor
b	blower
C	Solar geometrical concentration factor [–]
COP	Coefficient of performance [–]
c_p	Air constant p specific heat capacity [J kg^{-1} $°C^{-1}$]
D	Inner diameter of the receiver tube [m]
D_h	Hydraulic diameter [m]
e_w	Tube wall thickness [m]
F'	Collector efficiency factor [–]
F_R	Collector heat removal factor [–]
f	Darcy friction coefficient [–]
G_{bn}	Normal beam irradiance [W m^{-2}]
G_{bT}	Normal to aperture area beam irradiance [W m^{-2}]
h_a	Air heat transfer coefficient [W m^{-2} $°C^{-1}$]
IAM	Incidence angle modifier [–]
i	Specific enthalpy [J kg^{-1}]
K	Concentrated pressure losses coefficient [–]
k	Thermal conductivity [W m^{-1} $°C^{-1}$]
L	Length of the receiver tube [m]
L_c	Length of the collector mirrors [m]
L_{nc}	Length of the connection piping [m]
L_h	Characteristic heating length in the receiver tube [m]
$\dot{m}$	Air mass flow rate [kg s^{-1}]
$\dot{m}_{T_{ou}}$	Air mass flow rate for the specified T_{ou} [kg s^{-1}]
n	Supply tube
P	Receiver tube cross-section perimeter [m]
Pr	Prandtl number [–]
p	Pressure [Pa]
$\dot{Q}$	Thermal power [W]
$\dot{q}_s$	Incident concentrated solar irradiance [W m^{-2}]
$\dot{q}_u$	Useful thermal power flux [W m^{-2}]
Re	Reynolds number [–]
R_g	Gas constant = R/M_g [m^2 s^{-2} $°C^{-1}$]
R_p	Pumping ratio [–]
Sl	Slenderness parameter [–]
T	Temperature [K]
U_L	Thermal losses overall coefficient [W m^{-2} K^{-1}]
v	Average airflow velocity [m s^{-1}]
$\dot{W}$	Power [W]
W_a	Rectangular aperture total width [m]

Greek

φ	Extended surface coefficient [–]
γ	Isentropic exponent [–]
η_{op}	Optical efficiency [–]
$\eta_{r,SAH}$	Receiver efficiency of SAH [–]
$\eta_{r,TSAH}$	Receiver efficiency of TSAH [–]
η^*_{SAH}	Efficiency of SAH [–]
η_{eg}	Averaged electricity generation efficiency [–]
η_m	Mechanical efficiency turbocharger coupling shaft [–]
η^*_{TSAH}	Efficiency of TSAH [–]
η_{tt}	Total to total isoentropic efficiency [–]
η_{TC}	Turbocharger global efficiency [–]
π	Pressure ratio [–]
θ	Non-dimensional temperature [–]
μ	Dynamic viscosity [kg·m^{-1}·s^{-1}]
ν	Kinematic viscosity [m^2 s^{-1}]
ρ	Density [kg m^{-3}]

Subscripts

a	Air
amb	Ambient
atm	Atmospheric
b	Blower
c	Compression
d	Delivery to user
e	Expansion
em	Electro-mechanical
ex	Receiver tube external surface
f	Friction
in	Receiver inlet
k	Kinetic energy component
m	Average along the receiver
max	Maximum
min	Minimum
n	Outlet of supply tube to receiver
ou	Receiver outlet
p	Polytropic, pumping
R	Recirculation, over-pressure
r	Receiver
ref	Reference turbomachine
t	Total or stagnation variable
Tou	At outlet temperature
ts	Total to static
u	Useful
w	Wall
$\dot{W}=0$	Mechanical balanced operation
0	Inlet from atmosphere
1	Compressor inlet
2	Compressor outlet
$2n$	Receiver entrance TSAH
3	Turbine inlet
4	Turbine outlet

Acronyms

EU	European Union
HTF	Heat transfer fluid
H&C	Heating and cooling
IAM	Incident Angle Modifier
LFC	Linear Fresnel collector
OAC	Open-air circuit
PTC	Parabolic Trough collector
PV	Photovoltaic
SAH	Solar air heater
SHC	Solar heating and cooling
SHIP	Solar heat for industrial processes
TSAH	Turbo-assisted solar air heater

Others

$\langle\ \rangle$	Functional dependence

1. Introduction

The simultaneous increase in world population, development, and the enhancement in living standards has driven a growing demand for energy and it is projected to increase in the coming years, according to the International Energy Outlook [1], the International Energy Agency [2], and the BP Energy Outlook [3]. On the other hand, fossil fuel consumption, such as oil, natural gas, and coal, leads to greenhouse-effect and air pollutant emissions in the atmosphere that have raised concerns about climate change [4], and local health hazards. At the same time, increased consumption of fossil fuels leads to shortages and also can lead to price instabilities and geopolitical conflicts. The adverse environmental effects and safety issues of fossil fuel consumption strengthen the suitability of renewable energy sources and give them a unique opportunity to develop and grow. Among renewable energies, solar energy, the most abundant source of renewable energy on the planet, attracts the most attention. Many studies have been accomplished on methods of using Solar energy for Heating and Cooling (SHC) (please see the Symbol List), [5], in a program by the International Energy Agency, and on a review by Wang et al. [6], among others. Solar Electricity production and in particular by PhotoVoltaic means (PV) is also investigated, e.g., [7], as well as thermo-solar solutions [8]. As one of the most significant energy consumptions in developed countries corresponds to heat demand, both in buildings and industries, solar energy for obtaining heat is one of the priorities in research policies, either from the European Commission [9], by Solar Heat Europe [10], and the European Technology Platform on Renewable Heating and Cooling [11]. Obtaining heat from solar energy can be performed by using technologies that spread from very simple, even using local expertise and local materials, up to high tech setups, some of them now in development.

According to the European Commission [9], Heating and Cooling (H &C) represent 46% of the European Union (EU) energy needs. The EU industry uses 70.6% of its energy consumption (193.6 Mtoe) for space and industrial process heating, and still, 84% of H&C is generated from fossil fuels, while renewable energy generates only the remaining 16%. The European Strategy plan for H&C [12], states that 45% of energy for heating and cooling in the EU is used in the residential sector, 37% in industry and 18% in services. Heat for industry covers a broad temperature range. Metallurgy applications use heat above 1000 °C, and ambient thermal comfort requires only about 30 °C. Researchers recognize at least three temperature intervals: i) the high-temperature range above 1000 °C, ii) the low-temperature range below 100 °C, and iii) the medium temperature applications that lie in between them.

Farjana et al. [13], reviewed the Solar Heat for Industrial Processes (SHIP) state of art and potential. They analyzed the industrial heat demand by sectors, identifying the processes requiring low and medium temperature heat. They also found that the majority of the existing SHIP installations are in the low-temperature range, manly using flat plate collectors, air collectors, and evacuated tube collectors. Kalogirou in [14], states that the temperature requirements of SHIP application ranges are 60 °C to 260 °C. According to [15], around 50% of the energy consumption by industry is used for producing heat below 400 °C. They state that almost 50% of heat demand in the industrial sector can be potentially fulfilled by solar energy thanks to the advanced solar process heat technologies, able to provide temperatures up to 400°. Concentrating solar technology shows great potential as medium temperature heat source for industry, [16], among others. Several studies report that SHIP facilities using concentrating technology can be a financially competitive option [17], even cheaper than fossil fuel-based solutions [18], and [19].

1.1. Solar hot air for industrial processes

In [20], industrial processes using air as heat transfer medium are reported up to 1500 °C, but more currently up to about 225 °C. A

Table 1
Some examples of industrial process heat with hot moderate pressure air.

Distillation and evaporation	Thermal processing	Curing/backing	Residues processing	Plastics and rubber processing
Drying, e.g., paper, seeds and grains, leaves, ceramics, mining products, timber. Biomass.	Preheating of combustion air. Preheating before expansion in CAES	Painted products, pharmaceutical drugs	Waste sludge drying, e.g., Blackwater sediments, olive oil residues. Brine spray evaporation. Ash dewatering	Separation, drying, melting and soldering of plastics
Foods drying/processing/cooking e.g., dry milk/coffee production	Fabric clothes ironing/dying/scouring. Torrefaction	Wood superficial treatment	Anaerobic digester water heating by bubbling	Shrinking of plastic sleeves. Vacuum plastic sheet forming

common application of hot air is convective drying. Drying devices are very energy-demanding, especially when the purpose is dehydrating or dewatering due to the high latent heat of water evaporation, [21]. According to [22], the utilization of a high amount of energy in the drying industry makes it one of the most energy-intensive operations, with a crucial industrial relevance. Among a variety of techniques, hot air convective drying is much used, frequently configured as Open to Atmosphere Circuits (OAC). As a result, [23], reports that industrial dryers consume about 12% of the total energy used in manufacturing processes and the drying cost may rise to 60 to 70% of the total product cost. Further data on convective drying is given by [24]. A plethora of drying methods and drying equipment is reported in [25], among others. Hot air convective drying in [26], and additionally, freezing in [27], both highlight the importance of drying for food processing. Mekhilef [16], and Lillo-Bravo [19], provide further information on solar drying potential in industries. Since the application of hot air in industries is very diverse, reviewing all cases is beyond the scope of this article. Table 1 offers a short overview.

In industries, hot air is frequently produced by direct electrical heating, which is very intensive in primary energy consumption. The direct use of combustion fumes instead of atmospheric air is also widespread [20]. More elaborated processes use a Heat Transfer Fluid (HTF) of high heat transfer and carrying capacities, such as diathermic oils or steam, to produce hot air on-site from fossil fuel or biomass combustion.

Hot air can be produced by solar energy directly using solar air collector, in the low-temperature range [13]. Indirect solar air heating using flat plates collectors, evacuated tube collectors, or concentrating collectors, require a HTF to absorb, transport, and transfer solar heat to air, typically through a liquid/gas heat exchangers. Linear concentrating collectors, either Parabolic Trough Collectors (PTC) or Linear Fresnel Collectors (LFC), allow higher driving temperature than other collectors but a proper HTF, as thermal oil, hot pressurized water, or steam is needed. Using conventional HTFs is very convenient but complicates the facilities. One of the main advantages of liquid HTFs is their capacity of limiting the temperature of the collector receiver wall, thus protecting the optically selective coating. Nowadays, diathermic oils in thermo-solar power plants, based on linear concentrating collectors, have reached up to 300 °C maximum operating temperature, according to the above-cited references, and it is expected to reach 425 °C within acceptable degradation. The favorable heat-carrying capacity of diathermic oil implies an average wall temperature of the receiver tube about 20 °C above these values. Besides, peripheral temperature differences of about 20 °C were found [28], although this depends on the peripheral homogeneity of the irradiance impacting on the tube surface. In [29], the use of molten salts inside LFCs is proposed up to 550 °C just by using a Cermet optically selective coating in the absorber tube. The even higher heat transfer capacity of molten salts would imply wall temperatures up to 600 °C. With water as HTF, both boiling and especially freezing during nights are problematic; besides that, thermal expansion and vapor pressure above 100 °C imply a specific technology, not mentioning corrosion and scale. Despite the complications of two-phase flows, boiling and later condensation of water configures a highly energy-intensive heat-carrying process that can be very attractive, justifying the widespread use of industrial steam. With diathermic oils and concerning internal pressure, high temperatures up to 500 °C are possible with no problem. However, odors, burns, fire risk, and cost are inconvenient issues for industrial applications.

Pietruschka et al. [30], demonstrates a plant for powder milk production using solar air at 185 °C. There, diathermic oil flows through solar collectors producing steam with a boiler, which in turn produces hot air with a condensing heat exchanger. The same reference describes another demonstration plant, where ceramics is dried/cured in a range of 200 °C to 260 °C, driven by solar steam to air condensing heat exchangers. A direct medium temperature solar dryer is presented in [31], using PTCs delivering air at 280 °C at 2 bar, although 330 °C seemed optimal. It is worth noting that this configuration avoids conventional high heat-carrying capacity HTFs.

1.2. Direct solar air heating framework

Heating air directly inside a solar collector seems attractive for being the air cost-free, non-toxic, and pressure compliant. Conventional Solar Air Heaters (SAH) rarely have been used for medium temperature applications, and mostly their usage has been restricted to the low-temperature range for indoor ambient air heating as well as for drying food derivatives [32], for transpired SAHs. This is the general practice, Saxena et al. [33]. Kumar et al. in [34], indicate the nowadays progress of SAHs, confirming the practice. Direct air heating inside concentrating collectors enables to produce medium temperature air avoiding the use of the expensive HTF as well as the liquid/gas heat exchanger, improving the feasibility of solar hot air facilities in industry.

It seems justifiable introducing the direct production of solar hot air at medium and high temperatures, using commercial concentrating linear solar collectors like the ones mentioned in [35], but improving the performance beyond. There are three main problems, 1) the heat capacity per unit volume $c_p\rho$ of air is low, 2) the atmospheric air density ρ is low implying high velocities for a given mass flow rate $\dot{m}$, 3) the thermal conductivity is low [36], has investigated this issue in detail.

Low heat capacity per unit of volume results in a higher volume flow rate compared to a liquid HTF in order to limit the end temperature for a given installation size. The low density of air originates high mean velocity when a substantial mass flow passes inside the receiver tube. As consequence, high stagnation pressure losses originated across the tube length, resulting in a high pumping power required to circulate air through the installation. For long layouts, pumping power required could result in the same order of magnitude of solar power gain. The low density can be alleviated by using a high pressure. However, the issue of which combination of velocity $v$and tube diameter D can be used does not seem to be clearly presented in the open literature neither their interaction with the concentrated irradiance impacting on the receiver $\dot{q}_s$.

On the other hand, air internal heat transfer is modest. Low density ρ 1 to 10 kg m^{-3} combined with the viscosity of air $\mu = 29.6$ mPa s originates a high kinematic viscosity of $\nu = \mu\rho^{-1} = 48 \times 10^{-6}$ m^2 s^{-1} at 1 bar and 300 °C, two orders of magnitude greater than water. Generally, air shows a slight disadvantage in term of Reynolds number of the flow inside a collector receiver tube of diameter D, $Re = Dv\nu^{-1}$ which leads to a potentially low turbulent heat transfer coefficient $h_a \propto Re^{0.8}$ [37]. A low h_a turns into a high-temperature difference with the receiver tube wall ΔT_w, which simultaneously absorbs the solar radiation and transmits heat to the inner flowing air. This leads to high wall operating temperature, eventually surpassing the threshold temperature allowable by solar receiver tube. Commercial stainless-steel tubing can easily withstand the up-to-now considered receiver tube temperatures. However, the external optically selective coating, although under vacuum, degrades with excessive temperatures. Zu at al., in [38], states that the selective coating of absorber tubes are typically limited to 450 to 550 °C assuming a 20 to 30 years lifetime, according to manufacturers, e.g., [39], and [40]. Because of these limits, and considering the interest of higher temperatures for the upcoming developments in thermo-solar power plants, 600 °C can be considered as a maximum threshold temperature when producing solar hot air for a development that would yield commercial units shortly. Low h_a can be compensated by using extended internal surfaces such as fins or pins, so that reducing the maximum wall temperature. Longitudinal internal fins in PTC receiver tubes operating with gases has been studied by [41]. Simulating direct air, helium and carbon dioxide heating, they found that fins improve thermal efficiency although they introduce higher stagnation pressure drops. Increasing the operating mass flow rate also is beneficial on h_a, although the increased velocities translate

into higher stagnation pressure drops and greater pumping power consumption. Another technology tries to avoid surpassing the wall temperature limit using gases; cavity or volumetric receivers are proposed instead of linear concentrating geometry, e.g., [42], with coiled tubes, [43], with enhanced surfaces, and in some cases including tubular cavity receivers [44]. Nowadays, these solutions do not seem to be commercial. Concerning tube wall temperature, an inhomogeneous distribution causes tube bending [45]. When the tube touches the external glass envelope, breakage is possible. Thus, procedures to better distribute the concentrated irradiance and even some structural modifications to limit bending seem necessary. Therefore, a secondary optics seems favorable so that slight defocusing allows a more uniform distribution.

In [46], both a theoretical and experimental study was set up to confirm the feasibility of high temperature and high-pressure gas solar heating using linear concentrating solar collectors. They indicate that the latest developments on receiver tubes and selective coating provide tubes with a wall temperature limit of 550 °C, while the pressure can be kept up to 100 bar [29]. Solar superheating of steam has also been studied, using PTCs, e.g., [47], although at outlet fluid temperatures limited to a moderate 375 °C. Their 3D mathematical model showed a mean temperature difference of 16 °C between steam, at 60 bar, and wall. In [48], supercritical CO_2 was theoretically explored as HTF inside a PTC, being more favorable than air for direct solar heating. Bellos [49], performed an energetic and exergetic comparison of various gases as working fluids in a PTC. Air, nitrogen, carbon dioxide, helium, and argon were analyzed in order to determine the best working conditions for each gas.

Air as a HTF in concentrating collectors has been studied in the framework of the solar Brayton cycle. Reaching a competitive efficiency of a solar Brayton cycle for power production requires air temperatures in the range of 600–1.000 °C [50], which cannot be reached inside linear concentrating collector, as mentioned above. Nevertheless, concentrating collectors have been combined with a combustion chamber to power a Brayton cycle in solar-assisted gas turbines, as in [51]. Recently, Cinocca et al. [52], studied a complex Brayton cycle for electricity production using hot air with PTCs at 30 bar of pressure. The cycle is configured with intercooled (4 stages) compression and reheated expansion (2 stages) using solar heat; in fact, a kind of discrete steps Ericsson cycle. Regeneration is performed before solar heating, at the compression stages exit. Inlet and outlet are at atmospheric pressure; thus, it is an OAC. An external heater fed by biomass boosts the solar air providing a nominal reheated air temperature increase from 540 °C to 580 °C of turbine inlet temperature.

As a conclusion of the open literature analysis, there is interest and needs of solarizing industrial processes, but those using hot air are just in their early stage of a massive introduction. It seems that using air as a heat-carrying fluid has high potential for some applications, but its possibilities have not been fully explored. Heating air at the upper limit of the range, 300 to 400 °C seems reasonable for increasing the energy density of the air and keeping some over-temperature to enhance heat transfer to the point of application, indicating a practical objective around 300 °C. If lower temperatures are needed, dilution options are possible.

This paper offers a theoretical study on the viability of directly producing hot air inside linear concentrating solar collectors, as the literature on this concept is scarce. It offers also optimizing parameters and performance figures.

1.3. Materials and methods

Up to this point, Section 1 indicates that the open literature is incomplete on the very interesting opportunities for producing heat for industry based on the direct heating of air. More precisely, this paper studies the technical viability of directly producing hot air using linear concentrating solar collectors in temperature ranges of 300–400 °C for its use in industrial processes. Two concepts are proposed and analyzed: a) heating atmospheric air in a direct solar air heater SAH described in Section 2, b) using an innovative proposal and layout that is a turbo-assisted solar air heater TSAH, presented in Section 3.

Section 2 insights into selected issues from the review presented above and endeavors a theoretical analysis for assessing the technology and establishing the design principles constrained by the effects of the basic parameters. It presents a 1D model of the solar collector, on the grounds of a well documented and tested methodology. The general simplifying assumptions of 1D models are uniform peripheral temperature distribution of the variables in a cross-section for a) receiver's tube wall, b) flow, and c) concentrated solar irradiance. A negligible heat transfer via conduction in the longitudinal direction is also assumed [55], among others. As 1D model governing equations are written in terms of derivatives in time and longitudinal space, longitudinal variations of the model forcing variables can be included, e.g., solar irradiance [53], and [54]. It is conventional to transform the partial differential equations system into lengthwise marching ordinary differential equations from the inlet to outlet of the tube, if the residence time of the fluid is much shorter than the characteristic time for external variables variations, such as the solar irradiance, which is generally fulfilled in practice. Integration is performed to obtain approximate solutions following the well-established methodology in [55], but here adapted to SAHs. There are classical studies on heat transfer of air flowing inside tubes, e.g., [56], corroborating the validity of the Dittus-Boelter correlation [37], for heat transfer inside tubes;

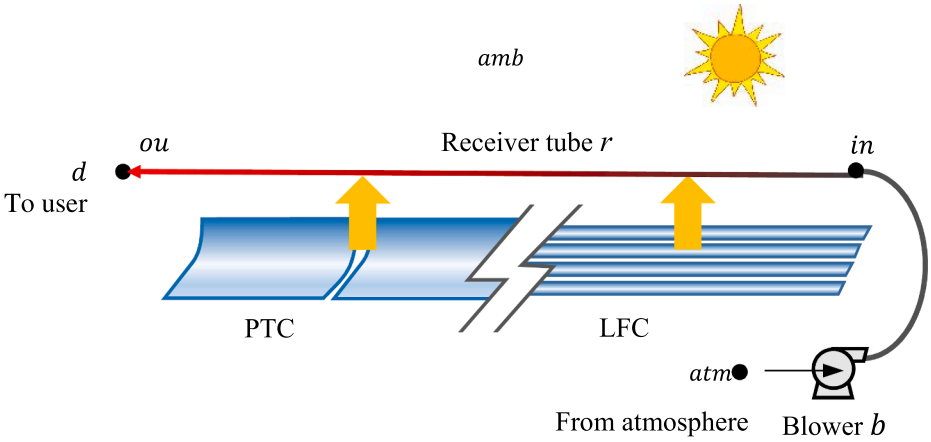

Fig. 1. Layout for direct SAH using concentrating linear collectors, here as open circuit configuration. The solar receiver tube is *r*; the blowing fan is *b*. PTC or LFC type collectors are possible so that a single line of a combination of them is shown.

thus it will be used for predicting the heat transfer coefficient between the tube wall and the air inside the tube h_a. Thanks to a set of simplifications, this section gives a clear view of the basics of the direct SAHs. A framework for evaluating the performance of simple SAH, meaning this, sending atmospheric air to the collectors, is provided in Section 2, pointing out the technical drawbacks that limit its feasibility within a defined range of design parameters and operating conditions. A novel non-dimensional slenderness parameter *Sl* arises, as a primary indicator of the layout of the linear concentrating solar collectors that are limited by the maximum wall temperature.

Section 3 introduces the innovative concept of using a turbocharger to implement a Turbo-assisted Air Heating (TSAH), already patented [57], which overcomes the main drawbacks of the simpler SAH. The principle of proposed TSAH is simple, as a higher atmospheric pressure is beneficial for reducing the pumping power inside the receiver tube, pressurization is incorporated. It turns out that the compressing power necessary would be excessive. The solution to this problem is to recover the pressurizing power by an expander; in fact, a turbine connected to the compressor, this way configuring a kind of turbocharger, Fig. 1. Engine turbochargers have been manufactured by millions, offering a mature and low-cost way of both pressurizing and expanding air at pressures below 4 bar [58]. The proposed layout configures an air solar Brayton cycle with a different purpose than its normal use as a prime mover [59]. Instead of producing power, it aims at producing heat carried by its outlet stream. In principle, the shaft shared by compressor and turbine would be freewheeling. The net mechanical power that can remain as overpressure at the outlet can be better used for pumping the hot air through the user facility instead of being recovered in an electric generator, although this is possible. Freewheeling gives an autonomous working condition for the turbocharger, eliminating the pumping power. Using the already introduced slenderness parameter *Sl* jointly with the overall turbocharger efficiency η_{TC} as the main parameters, the analysis gives the boundaries of the working space of the concept. In this paper, η_{TC} is assumed to be known, based on previous experience, and on references [58–77] so that the turbocompressor and turbine performance maps are not needed at this stage of the study of the concept, as only the design operating point is of interest.

Section 4 analyses the results given by the combination of the reduced-order models of the solar collector and the turbocharger to evaluate the concept. This section presents the performances of the TSAH concept under a broad range of design and operative parameters, either related to solar collectors or turbocharger, evaluating their combined effects. The study highlights the flexibility of the concept and identifies the optimal design options. A Conclusions section follows this section resuming the findings.

2. Effect of basic parameters on direct solar heating

As linear concentrating solar collectors, delivering medium or even high-temperature gases are not common nowadays, this section offers a simplified 1D analysis to establish a framework to asses the concept under study, aiming at LFCs and PTCs, according to [55].

Linear concentrating collectors typically are laid forming rows aligning several modules along their axis, summing up a length L_c. For industrial applications, it tends to be much smaller, L_c 10 to 100 m than for concentrating power plants, where L_c 100 to 1000 m. Several rows in parallel embrace the total mass flow rate. The single row mirror rectangular, of length L_c and with W_a, the aperture area is A_a. The beam fraction of the solar normal irradiance G_{bn}, impacting on the mirror aperture width W_a, is concentrated on the tube perimeter P_{ex}. This results in a concentrated irradiance on the receiver tube external surface $\dot{q}_s$, Eq. (1), according to the optical efficiency η_{op} and the geometric concentration C.

$$A_a = L_c W_a;\ \dot{q}_s = G_{bn}\eta_{op} C;\ C = W_a/P_{ex} \tag{1}$$

Optical efficiency $\eta_{op} = \eta_{op,max} IAM$ is characteristic of the collector considered, resulting from its design and manufacturing, besides to change with the orientation and sun position. With current technology, $\eta_{op,max}$ 0.5 to 0.8 varying from PTCs to LFCs. The Incidence Angle Modifier *IAM* is a correcting factor. For PTCs, the *IAM* includes the anisotropic optical properties variations, the cosine effect produced by non-null incident angle of sun rays with the reflecting surface normal, and end or tail effect, due to the reflected irradiance impacting away from the tube end or having some length of the receiver tube being non-illuminated [60]. For LFCs the determination of *IAM* is more complex, since blocking, mirrors mutual shadowing and eventually, secondary optics shadowing must be accounted for, in addition to the effects above mentioned for PTCs [61]. In order to hold general validity, this analysis does not explicitly consider them. All these effects can jointly be taken into consideration on the length averaged value of η_{op}. The following viability analysis have been performed considering a concentrated solar irradiance $\dot{q}_s$ as the relevant parameter, thus including η_{op},while the determination of its value as a result of the collector characterization is out of the scope of this work. A wide range of values of $\dot{q}_s$ are considered in the analysis in order to include either PTC and LFC types of different size, in a wide range of operating conditions and configurations (solar irradiance, orientation, sun position, *IAM*).

The circular receiver tube of diameter D has an external perimeter P_{ex}, while the internal wet perimeter P, is smaller as a result of a wall thickness e_w. The contact surface extension factor $\varphi \geq 1$, takes into account thin internal longitudinal fins, such that the cross-section A does not diminish appreciably. But the hydraulic diameter D_h decreases as the flow blockage of the fin thickness is considered negligible. Thus, the cross-section parameters are defined in Eq. (2).

$$P_{ex} = \pi(D + 2e_w);\ P = \varphi\pi D;\ A = \pi D^2/4;\ D_h = 4A/P = D/\varphi \tag{2}$$

Eq. (3) formulates the heat balance at any receiver tube cross-section. A heat transfer coefficient U_L determines the local heat losses from the receiver tube external wall, at a temperature T_w, toward the ambient at a temperature T_{amb}.

$$\dot{q}_s - U_L(T_w - T_{amb}) = \dot{q}_u \tag{3}$$

U_L depends on the geometry of the coaxial tubes and the materials; in general, it slightly grows with T_w. Due to the insulating effect of the evacuated glass tube surrounding the receiver tube, in addition to the selective coating, both convective and radiative losses to the ambient are minute. The PTCs and LFCs used for medium and high temperatures liquid HTFs show a relatively small value of the non-dimensional losses parameter, such that $U_L(T_w - T_{amb})/\dot{q}_s \ll 1$. To check its relevance for our case, [62], offers a model of thermal losses, according to the formulation in [53]. Based on that work, U_L is here considered constant, following typical values in the technical literature U_L = 3 to 6 W m^{-2} °C^{-1},[55]. A detailed thermal losses model of the solar tube is not needed for the screening of the technology. Thus, U_L = 5 W m^{-2} °C^{-1} will be used here as a reasonable value.

The net heat flux $\dot{q}_u$ is transferred from the wall at a temperature T_w toward the inner flow at bulk temperature T. Both are linked by the heat transfer coefficient of the inner air h_a, Eq. (4).

$$\dot{q}_u = \frac{h_a P(T_w - T)}{P_{ex}} \tag{4}$$

h_a can be expressed by the Dittus-Boelter correlation [37], Eq. (5), where the Reynolds numbers is Re_{D_h} and the Prandtl number is Pr, where $\dot{m}$ stands for the mass flow rate.

$$h_a = \frac{k}{D_h} 0.023 Re_{D_h}^{0.8} Pr^{0.4};\ Re_{D_h} = \frac{4\dot{m}}{\mu\pi D\varphi} \tag{5}$$

Taking air properties from [63], although here dry air is considered for generality one finds that $Pr = \mu c_p/k$ changes very little with temperature and humidity. At p = 1 bar, it increases from a minimum value of Pr = 0.698 at T = 200 °C up to 0.722 at T = 600 °C, and at

$T = 400$ °C, it increases from $Pr = 0.707$ at $p = 1$ bar to $Pr = 0.714$ at $p = 10$ bar. Heat conductivity increases monotonically with temperature, from $k = 38.25$ mW m^{-1} °C^{-1} at $T = 200$ °C, $p = 1$ bar up to $k = 61.14$ mW m^{-1} °C^{-1} at T = 600 °C, not changing appreciably from 1 to 10 bar. There is a relation between k and μ for gases, but somehow complex; the effects of p and T result in a cancelling effect on h_a, as μ grows also with temperature and not with pressure in the range of interest, from $p = 1$ to 10 bar. $\mu = 25.73$ μPa s at $T = 200$ °C and $\mu = 38.25$ μPa s at $T = 600$ °C. Actually, $k\mu^{-0.8}$, needed for Eq. (5), changes from 2.85 at $T = 200$ °C to 3.31 at $T = 600$ °C with the indicated units, just a bare 14% increase. Consequently, it seems that taking an average h_a along the tube length does not imply much error, despite the substantial air temperature increase.

Eq. (6) indicates the air gas constant R_g and the constant pressure specific heat capacity c_p, taken from [64], for the ideal gas, whose equation of state is $p/\rho = R_g T$, as well as the isentropic exponent γ.

$$\frac{c_p}{R_g} = 3.65 - 1.339\theta + 3.292\theta^2 - 1.913\theta^3 + 0.277\theta^4;\ \theta = \frac{T}{727\ °C} < 1;\ R_g = 287.1\ \text{m}^2\ \text{s}^{-2}\ °\text{C}^{-1};\quad \gamma = \left(1 - \frac{R_g}{c_p}\right)^{-1} \tag{6}$$

Following Eqs. (4) and (5), for a given solar net heat flux $\dot{q}_u$, $\dot{m}$ and D mainly determine T_w for a given T. The wall temperature T_w is maximum at the exit of the tube$T_{w,ou}$, so this constitutes a limiting point. p, T, and ρ do not appreciably influence the wall over-temperature ΔT_w as Eq. (7) shows simplified for $e_w \ll D$. This equation also shows the beneficial effect of φ in limiting ΔT_w, especially on the last downstream tube.

$$\Delta T_w = T_w - T = \frac{\dot{q}_u}{0.023\varphi^2 \frac{k}{D} Re_{D_h}{}^{0.8}\, Pr^{0.4}} \frac{D_{ex}}{D} \propto \approx \frac{\dot{q}_s}{\underbrace{\left(\frac{\dot{m}^{0.8}}{D^{1.8}}\right)}_{\approx(\rho v)^{0.8}} \varphi^{1.2}} \tag{7}$$

Eq. (7) indicates that ΔT_w is mainly dependent on the Reynolds number of the flow, which depends on $\dot{m}$ for a given tube diameter. For the low density of the gas compared to a liquid HTF, the mass flow rate which can be obtained at reasonable velocities inside the tube leads to much higher ΔT_w. A high length-average wall temperature $T_{w,m} = (T_{w,in} + T_{w,ou})/2, T_{w,ou} > T_{w,max}$ reduces the collector efficiency; in addition to that, an excess of thermal enlargement of the tube material will occur, which causes mechanical stress on the glass cover and tube junctions. Moreover, the downstream tube suffers the highest temperature; an excessive temperature would lead to deterioration of the selective coating. According to the technical literature, above mentioned, $T_{w,\max} \leq 450$ °C to 600 °C.

As a result of the 1D model, and following [55], the total solar heat power $\dot{Q}_u$ is according to Eq. (8).

$$\dot{Q}_u = P_{ex} \int_0^L \dot{q}_u \mathrm{d}x \tag{8}$$

$\dot{Q}_u$ can be expressed in terms of T_{in}, T_{ou} and T_{amb} alone, Eqs. (9) and (10). Eq. (11) introduces the collector efficiency factor F', using Eq. (5) to obtain the last term. Eq. (12) illustrates the origin of the heat dissipation factor F_R [55], which relies on constant U_L, h_a, $\dot{q}_s$, and fluid properties, along L. L_c and the receiver tube length L are assumed equal. The stagnation conditions are indicated as $_t$.

$$\dot{Q}_u = F_R L P_{ex} [\dot{q}_s - U_L(T_{in} - T_{amb})] = \dot{m}(i_{out} - i_{int}) \tag{9}$$

According to current practice, enthalpy is approximated using a temperature varying c_p with not a substantial error [65], among others, which allows explicating pressures and temperatures with both turbomachines and solar collectors, Eq. (10).

$$\dot{Q}_u = \dot{m}(i_{out} - i_{int}) \cong \dot{m}(c_{p,ou} T_{out} - c_{p,in} T_{int}) \tag{10}$$

The connection between wall and flow temperature is given by the collector efficiency factor F', [55], here including that $P_{ex} > P$, Eq. (11).

$$F'\langle\dot{m}\rangle = \frac{\dot{q}_s - U_L(T_w - T_{amb})}{\dot{q}_s - U_L(T - T_{amb})} = \left[1 + \frac{U_L P_{ex}}{h_a \langle\dot{m}\rangle P}\right]^{-1} \tag{11}$$

The lengthwise constancy of the parameters involved allows obtaining an analytical expression of F_R integrating the temperature from the tube inlet $x = 0$ where $T = T_{in}$ to the outlet $x = L$ where $T = T_{ou}$, Eq. (12), following [55]. An average specific heat $c_{p,m}$ is used.

$$F'\langle\dot{m}\rangle P_{ex} \mathrm{d}x = \frac{\dot{m} c_{p,m} \mathrm{d}T_t}{[\dot{q}_s - U_L(T - T_{amb})]} \Rightarrow F_R\langle\dot{m}\rangle = F'\langle\dot{m}\rangle \frac{L_h\langle\dot{m}\rangle}{L}\left[1 - \exp\left(-\frac{L}{L_h\langle\dot{m}\rangle}\right)\right] \tag{12}$$

L_h is a characteristic heating length, Eq. (13). The dependence of h_a, F', L_h and F_R on mass flow rate $\dot{m}$ is indicated in Eqs. (11), (12) and (13).

$$L_h\langle\dot{m}\rangle = \frac{\dot{m} c_{p,m}}{F'\langle\dot{m}\rangle P_{ex} U_L} \tag{13}$$

The thermal efficiency of the receiver tube $\eta_r$can be formulated as a compact expression using Eqs. (9) to (13), resulting in Eq. (14). T_{amb} can be slightly different to the atmosphere temperature T_{atm} owing to the sky and ground effective temperatures.

$$\eta_r = \frac{\dot{Q}_u}{\dot{q}_s P_{ex} L} = F_R\langle\dot{m}\rangle\left[1 - \frac{U_L(T_{in} - T_{amb})}{\dot{q}_s}\right] \tag{14}$$

2.1. SAH assessment

The basic equations stated above allow a general analysis considering an OAC layout of a SAH, shown in Fig. 1. Outlet air at the collector exit (ou) is delivered to the user (d). Thus, the outlet temperature T_{ou} is one of the most relevant parameters, being in this basic configuration $T_d = T_{ou}$. The effect of the blower, b in Fig. 1, over the inlet receiver temperature, is addressed as in Eq. (15), where v_{in} stands for the average velocity at the tube inlet and W_p stands for the pumping power to the flow.

$$T_{in} = T_{int} - \frac{v_{in}^2}{2c_{p,in}} = T_{atm} + \frac{W_p}{\dot{m} c_{p,p}} - \frac{v_{in}^2}{2c_{p,in}} \tag{15}$$

Combining Eqs. (10) to (13) determines the mass flow rate $\dot{m}_{Tou}$, Eq. (16), which ensures the desired outlet temperature T_{ou}, for a given $\dot{q}_s$, and a non-dimensional slenderness $Sl = L/P_{ex}$. For a given $\dot{q}_s$, L determines the total magnitude of $\dot{Q}_u$, while P_{ex} is determined by D_{ex}, Eq. (1). This diameter is usually limited to the commercially available evacuated tubes for cost-consciousness; thus, it is fixed for the model runs performed, Table 2. In Eq. (16) the enthalpy difference approximation of Eq. (10) has been included.

Table 2
Parameters common to the different simulation cases.

$T_{amb} = T_{atm}$	p_{atm}	D	D_{ex}	U_L	φ	D_n	K_n	L_{nc}
10 °C	1.013 bar	0.066 m	0.07 m	5 W m^{-2} °C^{-1}	1.0	D	2.0	6 m

$$\frac{\dot{q}_s c_{p,m}}{U_L}\left[1-\exp\left(-\frac{Sl D_{ex}^2 \pi^2 U_L}{\left(1+\frac{U_L D_{ex}}{h_a D}\right)\dot{m} c_{p,m}}\right)\right]\left(1-\frac{U_L(T_{in}-T_{amb})}{\dot{q}_s}\right) = c_{p,ou}T_{out} - c_{p,in}T_{int} \quad (16)$$

2.1.1. Minimum non-dimensional slenderness Sl

High values of Sl means, for the available values of P_{ex}, long collector rows, which are customary for a high $\dot{Q}_u$ at the design point of operation. They require large $\dot{m}$ for limiting T_{ou}. On the other hand, small collector lengths, typical for small $\dot{Q}_u$, require low $\dot{m}$ for reaching the same T_{ou}. Besides controlling air temperature, $\dot{m}$ determines the ΔT_w, Eq. (7), and the highest wall temperature $T_{w,ou}$, which happens at the tube outlet. Therefore, a small collector working with low $\dot{m}$ and high $\dot{q}_s$ can overcome the receiver thermal limits $T_{w,max}$. For a given T_{ou} and $\dot{q}_s$, the minimum mass flow rate $\dot{m}_{min}$permitted by the thermal limit can be obtained by solving Eqs. (3) and (7) for $T = T_{ou}$ and $T_w = T_{w,max}$, as in Eq. (16).

$$\dot{m}_{min} = \frac{\mu \pi D \varphi}{4}\left(\frac{\dot{q}_s - U_L(T_{w,max}-T_{amb})}{0.023(T_{w,max}-T_{ou})\varphi^2 \frac{k}{D} Pr^{0.4}}\right)^{1.25} \quad (17)$$

Introducing $\dot{m}_{min}$ of Eq. (17) into Eq. (16), $T_{w,max}$ and T_{ou} give a compact condition, which determines a minimum allowable Sl_{min} for any $\dot{q}_s$, Eq. (18).

$$\frac{\dot{q}_s c_{p,m}}{U_L}\left[1-\exp\left(-\frac{Sl_{min} D_{ex}^2 \pi^2 U_L}{\left(1+\frac{U_L D_{ex}}{h_a D}\right)\dot{m}_{min} c_{p,m}}\right)\right]\left(1-\frac{U_L(T_{in}-T_{amb})}{\dot{q}_s}\right) = c_{p,ou}T_{out} - c_{p,in}T_{int} \quad (18)$$

For the simulation cases in this paper, Table 2 indicates the parameters used.

Fig. 2 depicts Sl_{min} versus $\dot{q}_s$for several T_{ou} and $T_{w,max}$ of interest, considering the commercial standard tube diameter of Table 2. Sl_{min} is very small considering the highest thermal limits on the technical literature $T_{w,max}$ = 600 °C but can turn into a severe constraint to the feasibility of SAH for a less performing receiver tube, i.e. $T_{w,max}$ = 500 °C, and a high enough T_{ou}.

2.1.2. Pumping power

In addition to the modest value of h_a, another issue of direct SAHs is the power consumption for pumping the air with the blower through the receiver tube $\dot{W}_p$. The low heat volumetric capacity $c_p\rho$ of gases at low pressures, compared to a generic liquid HTF, leads to operating with a high mean velocity v to obtain the mass flow rate required to limit T_{ou}, as Eq. (10) indicates. Eq. (19) provides $\dot{W}_p$, neglecting any inlet pressure loss, considering the exit kinetic energy valuable, and a blower isentropic efficiency, total to total η_{ptt}. Eq. (19) also explicates the incompressible approximation. O⟨ ⟩ indicates an infinitesimal of the order indicated, in a Taylor series expansion for $\Delta p_t/p_{atm} < 1.0$. The pumping total to total isentropic efficiency assumed is η_{ptt} = 0.5.

$$\dot{W}_p = \dot{m} c_{p,p}(T_{int}-T_{atm}) = \dot{m}\frac{c_{p,p}T_{atm}}{\eta_{ptt}}\left[\left(1+\frac{\Delta p_t}{p_{atm}}\right)^{\frac{\gamma-1}{\gamma}}-1\right] = \dot{m}\frac{c_{p,p}T_{atm}}{\eta_{ptt}}\left[\frac{\Delta p_t}{p_{atm}}+\mathrm{O}\left\langle\left(\frac{\Delta p_t}{p_{atm}}\right)^2\right\rangle\right] \quad (19)$$

The required total pressure to be pumped $\Delta p_t = p_{int} - p_{out}$ results from the kinetic pressure change Δp_{kt} due to density variation and the friction pressure drop Δp_{ft}. For the sake of simplicity, one can consider an air density ρ_m at an average temperature, and neglect Mach number corrections owing to its low value. The friction term is modeled through the Blasius formulation using the Darcy friction factor f of turbulent flow inside smooth tubes [66], Eqs. (20) and (21). The Blasius formula is for smooth tubes but for the moderate Reynolds numbers happening, it seems accurate enough for drawn stainless steel tubes as can be checked in a Moody graph. K_n accouts for concentrated pressure losses due to bends and connections and L_{nc} is an additional pipe length needed to connect the blower with the solar tube, and the solar tube outlet with the delivery point, according to Table 2.

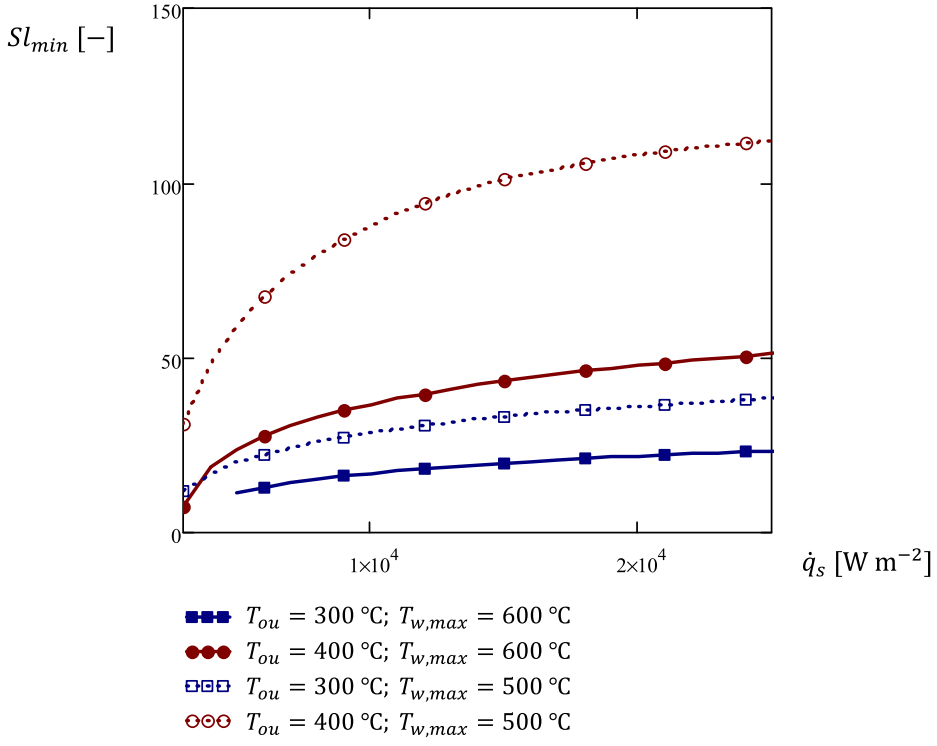

Fig. 2. Minimum slenderness parameter Sl_{min} of SAH versus concentrated solar irradiance $\dot{q}_s$ for different T_{ou} and $T_{w,max}$.

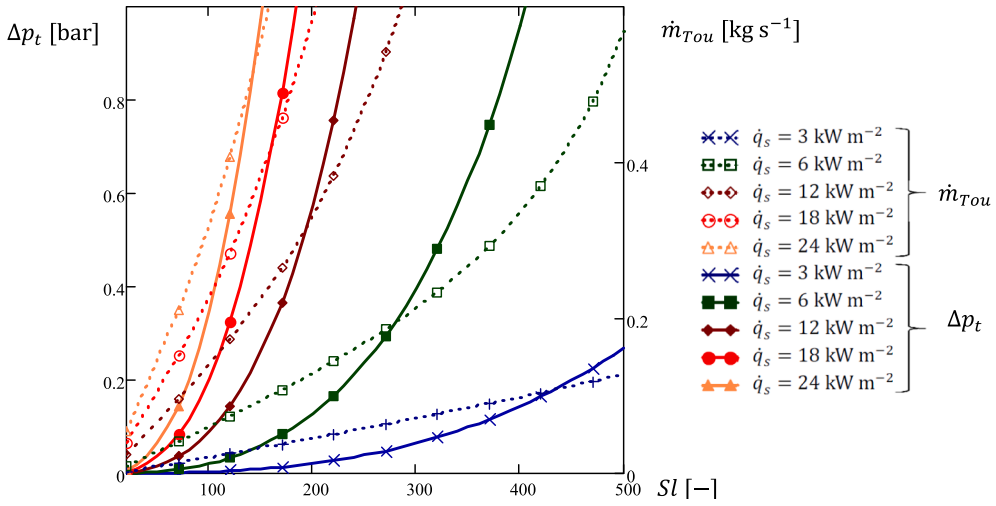

Fig. 3. Total pressure drop Δp_t and mass flow rate $\dot{m}_{Tou}$ versus $Sl = L/P_{ex}$ for T_{ou} = 350 °C.

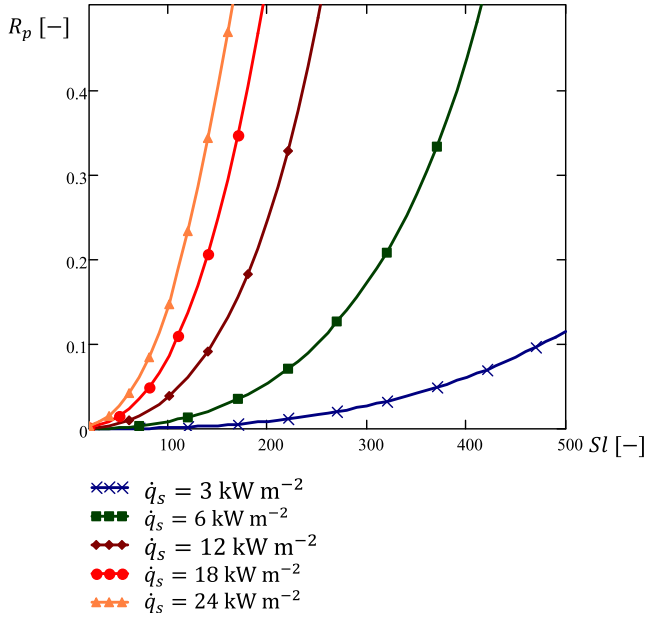

Fig. 4. Pumping ratio R_p versus $Sl = L/P_{ex}$ for several concentrated solar irradiances $\dot{q}_s$. T_{ou} = 350 °C.

$$\Delta p_t = \overbrace{\frac{1}{2}(\rho_{ou}v_{ou}^2 - \rho_{in}v_{in}^2)}^{\Delta p_{kt}} + \overbrace{\frac{1}{2}\rho_m v^2\left(f\frac{L\varphi + L_{nc}}{D} + K_n\right)}^{\Delta p_{ft}}$$
$$= \frac{1}{2}\left(\frac{4\dot{m}}{\pi D^2}\right)^2\left(\frac{1}{\rho_{ou}} - \frac{1}{\rho_{in}} + f\frac{L\varphi + L_{nc}}{\rho_m D} + \frac{K_n}{\rho_m}\right) \quad (20)$$

$$f = 0.316Re_{D_h}^{-1/4} \quad (21)$$

Introducing into Eq. (20) the mass flow rate $\dot{m}_{Tou}$ from Eq. (16), Δp_t can be estimated for several $\dot{q}_s$, varying Sl.

Fig. 3 shows Δp_t required by the SAH operating with a delivery temperature T_{ou} = 350 °C. The corresponding $\dot{m}_{Tou}$ obtained under the same conditions through Eq. (16) is also shown in Fig. 3. High $\dot{q}_s$ requires high $\dot{m}_{Tou}$ (to limit T_{ou} to the specified value), inducing high Δp_t, as a consequence of the high v, even for relatively small Sl. Instead, lower $\dot{q}_s$ allows to operates at moderate $\dot{m}_{Tou}$ and v also for long collector rows, L.

The pumping ratio $R_p = \dot{W}_p/\dot{Q}_u$ estimates the amount of external power needed to pump air inside the receiver tube over the solar power delivered to the flow. Eq. (22) provides the expression for R_p by combining Eqs. (16), (19) and (20). For a given T_{ou}, any Sl and$\dot{q}_s$, considering the mass flow rate $\dot{m}_{Tou}$, R_p can be determined for the same variables through Eq. (22).

$$R_p = \frac{c_{p,p}T_{atm}}{(c_{p,ou}T_{out} - c_{p,in}T_{int})\eta_{ptt}}\left[\left(1 + \frac{8\dot{m}_{Tou}^2}{p_{atm}\pi^2 D^4}\left(\frac{1}{\rho_{ou}} - \frac{1}{\rho_{in}} + 0.316\frac{Sl P_{ex}\varphi + L_{nc}}{\rho_m D}\left(\frac{4\dot{m}_{Tou}}{\mu\pi D\varphi}\right)^{-\frac{1}{4}} + \frac{K_n}{\rho_m}\right)\right)^{\frac{\gamma_p - 1}{\gamma_p}} - 1\right] \quad (22)$$

Fig. 4 shows the variation of R_p as a function of Sl for several concentrated solar irradiances $\dot{q}_s$. As $\dot{W}_p \propto \dot{m}^{(2\text{to}3)}$, highly concentrating collectors (high $\dot{q}_s$ under design point operation) operating at necessarily high $\dot{m}$ require high pumping powers, which can be in the same order of magnitude of the solar gain $\dot{Q}_u$.

Eq. (23) shows the dependence of both pumping power components on basic parameters, assuming for the moment the incompressible evolution in the blower to obtain analytical expressions. Typical values of $\rho_{in}/\rho_{ou} \approx 2$ from 10 °C to 500 °C imply that the kinetic total pressure loss $\Delta p_{kt} < \Delta p_{ft}$.

$$\dot{W}_{pk} \approx \dot{m}\frac{\Delta p_{kt}}{\rho_m \eta_{ptt}} \propto \dot{m}^3 D^{-4}\rho_m^{-2};\ \dot{W}_{pf} = \dot{m}\frac{\Delta p_{ft}}{\rho_m \eta_{ptt}} \propto \dot{m}^{2.75}L\rho_m^{-2}\mu^{0.25}D^{-4.75}\varphi^{1.25} \quad (23)$$

For a given $\dot{m}$, required for the above expressed thermal constraint, Eq. (23) shows that enlarging the tube diameter D is highly beneficial for decreasing $\dot{W}_p$. Besides this, it helps in limiting the tube bending from peripheral irradiance inhomogeneities, although this enlargement leads to higher P_{ex} and the associated growth of thermal losses, reducing the receiver thermal efficiency η_r. Tubes of larger D could be commercially available in the future as solar thermal power plants increase the PTC mirror width W_a from 6 to 8 or even to 10 m. The addition of internal fins, $\varphi > 1$, reduces $\Delta T_{w,ou}$, Eq. (7), but with the tradeoff of increasing $\dot{W}_p$, Eq. (19).

2.1.3. Direct heating efficiency

A direct heating efficiency parameter is η^*_{SAH}, Eq. (24). η^*_{SAH} does not take into account the optical efficiency η_{op}, considering as input source the solar power gathered by the receiver tube. Eq. (3). Pumping power is an additional power input to the SAH system, here assumed to be

provided by an electrically driven blower, Fig. 1. Since electricity is needed to run the blower with a total to total isentropic efficiencyη_{ptt}, the electrical pumping consumption is accounted for in terms of primary energy considering an average electricity efficiency, from primary energy to plug, of $\eta_{eg} \approx 0.15$to0.5. Here, an average value $\eta_{eg} = 0.42$ and an electro-mechanical pumping efficiency $\eta_{emp} = 0.95$ are chosen.

$$\eta^*_{SAH} = \frac{\dot{m}_{Tou}\,(c_{p,ou}\,T_{out} - c_{p,atm}\,T_{atm})}{Sl P^2_{ex}\,\dot{q}_s + \frac{\dot{W}_p}{\eta_{emp}\eta_{eg}}}; \tag{24}$$

$$\eta_{r,SAH} = \frac{\dot{m}_{Tou} c_{p,r}}{Sl P^2_{ex} U_L}\left[1 - \exp\left(-\frac{Sl P^2_{ex} U_L}{\dot{m}_{Tou} c_{p,r}\left(1 + \frac{U_L P_{ex}}{h_a P}\right)}\right)\right]\left[1 - \frac{U_L(T_{in} - T_{amb})}{\dot{q}_s}\right] \tag{25}$$

For $\dot{W}_p = 0$ the direct heating efficiency η^*_{SAH}equals the receiver solar efficiency η_r, evaluated from Eq. (14) under the same extreme temperatures and mass flow rate, referred to as $\eta_{r,SAH}$ in Eq. (25). Either η^*_{SAH} or $\eta_{r,SAH}$ can be calculated considering the system operating with the desired delivery temperature $T_d = T_{ou}$and $\dot{m}_{Tou}$ determined by Eq. (16), for any $\dot{q}_s$ and Sl. Fig. 5 shows results under the same conditions as in Fig. 3.

In Fig. 5, the direct heating efficiency η^*_{SAH}, for very small Sl, equals to $\eta_{r,SAH}$ owing to the negligible pumping power, but it decreases considerably as Sl grows. Thus, for slender collectors and according to the trend of $\dot{W}_p$ that Fig. 4 shows, η^*_{SAH} drops remarkably with Sl at highly concentrated irradiances, large $\dot{q}_s$. For small $\dot{q}_s$, the pumping power is lower so that η^*_{SAH} does not diverge remarkably from $\eta_{r,SAH}$. On the other hand, the receiver efficiency varies with $\dot{q}_s$. According to the principles of concentrating technology, collectors with higher concentration ratio C, thus larger $\dot{q}_s$, yield better thermal performances for having a smaller ratio $U_L(T_w - T_{amb})/\dot{q}_s$. Consequently, a direct air heating collector designed for small $\dot{q}_s$ needs a small pumping power, Fig. 4, even for large Sl but it carries the drawback of lower $\eta_{r,SAH}$, leading to modest η^*_{SAH}, which account for both effects. In order to operate with relatively high $\dot{q}_s$ and $\eta_{r,SAH}$, a possibility for reducing the high pumping power and avoiding the η^*_{SAH} drop arises considering Eq. (23). Besides depending on $\dot{m}$ and on D, $\dot{W}_p$ decreases quadratically with ρ_m. Thus, a moderate increase in ρ_m reduces pumping power remarkably, even for wide and long collectors with large $\dot{q}_s$ and Sl.The following section analyses a concept in this direction: the TSAH concept.

3. The model of the solar Brayton cycle for heat production TSAH

From the analysis performed in the previous section, direct air heating seems viable, up to medium temperatures, inside the receiver tubes of SAHs, Fig. 1. The thermal limit constraints exclude collectors with $Sl < Sl_{min}$, Fig. 2. Increasing Sl leads to high pumping power consumption, which discourages a long row. This worsens for large incoming heat flux, advising against a joint large aperture width W_a. Thus, a direct ambient air SAH is possible for moderate collector lengths and small W_a, assuming a) a lower heating efficiency due to a decreased receiver efficiency and b) power consumption for pumping air, i.e., through an electricity-driven blower.

For a given $\dot{m}$, an increase in inlet air density alleviates these drawbacks reducing both the kinetic and frictional components of the required external pumping power consumption $\dot{W}_p$. A strategy has to be found to reduce $\dot{W}_p$, indicated in Eq. (26). An increase of density from 2 to 4 times the ambient air density seems enough to reduce pumping power to reasonable values. Higher density would be beneficial, but inlet air temperature increase, due to adiabatic compression, limits the possible inlet compression ratios, indicated by Eq. (27).

The TSAH concept aims at recovering the compressing mechanical power by installing a turbine at the receiver tube outlet, which takes advantage of the larger air enthalpy, Fig. 6. Compressed air heated up to T_{ou} expands into a turbine that is mechanically coupled with the compressor, thus defining a Brayton cycle layout, here indicated as an OAC, although a closed-circuit layout is also possible. For the moderate T_{ou} allowed due to the receiver tube thermal limit, non-appreciable net mechanical power is expected at the turbocharger shaft, considering the viable efficiencies of single-stage radial turbomachines [50], but at least the freewheeling operation is the expected result. This way, high-density air circulating inside the receiver tube is achieved without any external energy consumption as air expansion at the turbine can provide both compressing and pumping power. Air exits the turbine at a medium temperature level, which is available for direct user applications, such as drying. Fig. 6 shows the layout, depicting two alternatives or combinations, PTC and/or LFC collector types. The hot air delivery temperature T_d doesn't coincide with T_{ou} as for SAH, Fig. 1, but with the air stream temperature at the turbine outlet $T_d = T_4$.

An auxiliary compressor or any external power is needed to turn the turbomachinery to a minimum speed to start. It also could avoid thermal damage to the receiver tube in case overheating is expected. A supply tube, n in Fig. 6, is required for sending the compressed air flow to the receiver inlet, of substantial length with a single row or an even number of them.

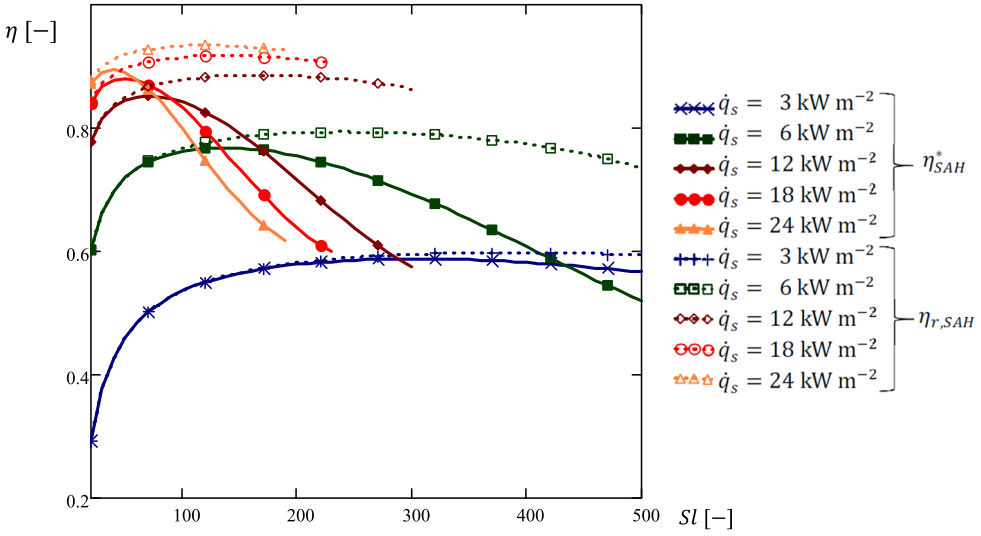

Fig. 5. Direct solar air heating efficiency η^*_{SAH} (solid line) and receiver efficiency $\eta_{r,SAH}$ (dashed line) versus $Sl = L/P_{ex}$ for different $\dot{q}_s$. $T_{ou} = 350$ °C.

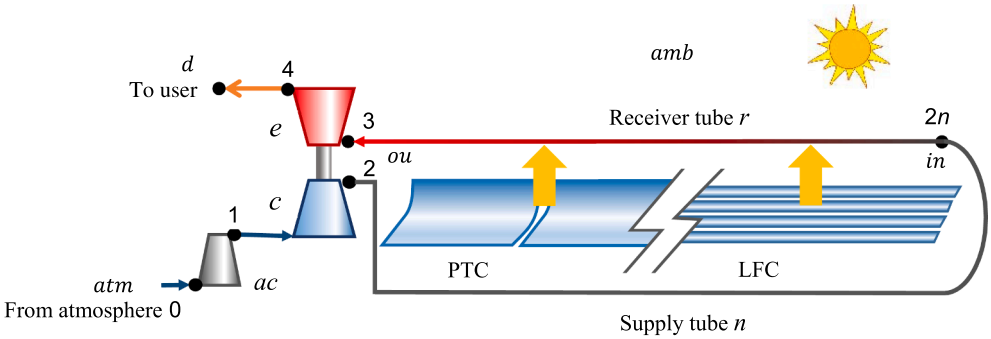

Fig. 6. Layout of TSAH using concentrating linear collectors, shown as an OAC Brayton cycle configuration. The solar receiver tube is *r*, the turbine is *e*, the compressor is *c*, the auxiliary compressor is *ac*, and the supply tube is *n*. Black dots indicate the cycle point.

3.1. TSAH modeling

Under the steady-state operation, the model excludes the auxiliary compressor; $p_{1t} = p_{0t} = p_{atm}$, and $T_{1t} = T_{0t} = T_{atm}$. Considering a total to total compression ratio $\pi_c = p_{2t}/p_{1t}$, atmospheric air is compressed up to p_{2t} and T_{2t} requiring a mechanical power $\dot{W}_c$ for a given isoentropic efficiency, total to total η_{ttc} and a pressure ratio π_c, as in Eq. (26), assuming perfect gas behavior through compression as well as through expansion.

$$\dot{W}_c = \dot{m} c_{p,c} T_{atm} \left(\pi_c^{\frac{\gamma_c - 1}{\gamma_c}} - 1 \right) \eta_{ctt}^{-1} \tag{26}$$

$$T_2 = T_{1t} \left[1 + \left(\pi_c^{\frac{\gamma_c - 1}{\gamma_c}} - 1 \right) \eta_{ctt}^{-1} \right] - \frac{v_2^2}{2 c_{p,2}} \tag{27}$$

The auxiliary tubes, as well as *n*, in Fig. 6, are thermally insulated so that the inlet temperature at the receiver is $T_{in} = T_{2n} \approx T_2$, $p_{in} = p_{2n} = p_{1t}\pi_c - \rho_{2n} v_{2n}^2/2 - \Delta p_{fnt}$, owing to the low Mach number. The frictional pressure drop in the supply tube follows Eq. (20), $\Delta p_{fnt} = \frac{1}{2}\rho_2 v_{2n}^2 (f\frac{L_n}{D_n} + K_n)$ where $K_n$is used for concentrated pressure drops due to bends. L_n corresponds to the collector length, L, plus an additional length L_{cn} that takes into account additional connection bends and piping, $L_n = L + L_{nc}$. Air exits the receiver tube at $T_3 = T_{ou}$ heated by a concentrated solar irradiance $\dot{q}_s$. The turbine inlet condition results as $T_{3t} = T_{ou} + v_3^2/2c_{p,3}$, at an stagnation pressure $p_{3t} = p_{2n} + \rho_{2n} v_{2n}^2/2 - \Delta p_{frt}$, where the total pressure drop inside the receivers both caused by friction and acceleration is, Eq. (28).

$$\Delta p_{rt} = \frac{1}{2}\left(\frac{4\dot{m}}{\pi D^2}\right)^2 \left(\frac{1}{\rho_3} - \frac{1}{\rho_2} + f\frac{L\varphi}{\rho_m D} \right). \tag{28}$$

The mechanical power provided by the expansion $\dot{W}_e$ can be calculated through the total to total efficiency η_{ett} and the total to total pressure ratio $\pi_e = p_{3t}/p_{4t}$ of the turbine, Eq. (29). Eq. (30) indicates the total outlet temperature T_{4t}.

$$\dot{W}_e = \dot{m} c_{p,e} T_{3t} \left[1 - \pi_e^{-\frac{\gamma_e - 1}{\gamma_e}} \right] \eta_{ett} \tag{29}$$

$$T_{4t} = T_{3t} \left[1 - \eta_{ett} \left(1 - \pi_e^{-\frac{\gamma_e - 1}{\gamma_e}} \right) \right] \tag{30}$$

The turbine delivers air at temperature, $T_d = T_4 = T_{4t} - \frac{v_4^2}{2c_{p,4}}$. The output pressure $p_{4t} = \pi_R p_{atm}$, where π_R indicates the pressure available bay the user. p_{4t} can be slightly larger than ambient pressure, depending on the operating variables and the performance of the turbine outlet diffuser. In what follows, $\pi_R = 1$is considered if it is not otherwise specified.

3.2. Freewheeling and the thermal limit

According to the proposed concept, the kind of turbocharger used for internal combustion engines [64], spins freely. In our case, this condition must be investigated. This is equivalent to null net power on its shaft $\dot{W} = 0$, thus from now on. Negative power at the shaft can occur during cloudy periods. Additional power could be supplied either by an external auxiliary compressor or by adding power to the turbocharger shaft, whatever is more convenient, in order to fulfill the user demand. Reheating using an external heat supply after the solar collector is another alternative.

Considering a mechanical efficiency of the turbo-compressor coupling shaft η_m,under steady-state operation, the freewheeling condition is achieved if Eq. (31) holds. Eq. (32) gives this condition detailing the basic parameters.

$$\dot{W} = \dot{W}_e \eta_m - \dot{W}_c = 0 \tag{31}$$

$$c_{p,c} T_{atm} \left(\pi_c^{\frac{\gamma_c - 1}{\gamma_c}} - 1 \right) = \underbrace{\eta_{ctt}\eta_{ett}\eta_m}_{\eta_{TC}} c_{p,e} \left(T_{ou} + \frac{v_3^2}{2c_{p,3}} \right) \left[1 - \left(\frac{\pi_c \left(1 - \frac{\Delta p_{nrt}}{p_{2t}} \right)}{\pi_R} \right)^{\frac{\gamma_e - 1}{\gamma_e}} \right] \tag{32}$$

Equation (32) does contain as operating parameters π_c, π_R, and the overall turbocharger efficiency $\eta_{TC} = \eta_{ctt}\eta_{ett}\eta_m$. The effect of total pressure drop $\Delta p_{nrt} = p_{2t} - p_{3t}$ along the supply and receiver tubes on the freewheeling operation $\dot{W} = 0$ can be noted. Eq. (33) details the total pressure drop in the supply and receiver tube. On the other hand, a high enough $T_3 = T_{ou}$ is needed in order to balance the pressure drop effect and provide the required compressing power. An expression for T_{ou} for a given *Sl* and $\dot{q}_s$ can be obtained from Eq. (16) considering $T_{in} = T_2$, Eq. (27), expressed in Eq. (34) for a single tube layout, as in Fig. 6.

$$\Delta p_{nrt} = \overbrace{\frac{1}{2}\left(\frac{4\dot{m}_{\dot{W}=0}}{D_n^2 \pi}\right)^2 \left(\frac{K_n}{\rho_2} + f\frac{SlP_{ex} + L_{nc}}{\rho_2 D_n} \right)}^{\Delta p_{nt}} + \overbrace{\frac{1}{2}\left(\frac{4\dot{m}_{\dot{W}=0}}{D^2 \pi}\right)^2 \left(\frac{1}{\rho_3} - \frac{1}{\rho_2} + f\frac{SlP_{ex}\varphi}{\rho_m D} \right)}^{\Delta p_{rt}} \tag{33}$$

$$c_{p,ou} T_{out} = \frac{c_{p,m}}{U_L} \left[1 - \exp\left(-\frac{SlF' D_{ex}^2 \pi^2 U_L}{\dot{m}_{\dot{W}=0} c_{p,m}} \right) \right] [\dot{q}_s - U_L (T_2 - T_{amb})] + c_{p,2} T_{2t} \tag{34}$$

The parameter $\dot{m}_{\dot{W}=0}$, indicated in Eqs. (33) and (34), stands for the freewheeling condition stated in Eq. (31), thus under turbocharger freewheeling. Considering Eq. (32) for a given η_{TC}, π_c and π_R, the maximum air temperature T_{ou} and the stagnation pressure drop along the tubes Δp_{nrt} determine the freewheeling condition. According to Eq. (34) the outlet receiver temperature T_{ou} is determined for any *Sl* and $\dot{q}_s$ by the air mass flow rate $\dot{m}_{\dot{W}=0}$. Solving Eq. (32) coupled with Eqs. (33) and (34), reveals the mass flow rate $\dot{m}_{\dot{W}=0}$ that verify the freewheeling condition for any *Sl* and $\dot{q}_s$, assuming constant η_{TC}, π_c and π_R.

Besides satisfying Eqs. (32) to (34), the operation must respect the

thermal limits of the receiver tube. Eq. (35) is obtained from Eqs. (3) and (4), providing an expression to verify $T_{w,ou} \leq T_{w,max}$.

$$T_{w,ou} = \frac{\dot{q}_s + T_{ou} h_a \langle \dot{m}_{\dot{W}=0} \rangle \frac{D}{D_{ex}\varphi} + T_{amb} U_L}{h_a \langle \dot{m}_{\dot{W}=0} \rangle \frac{D}{D_{ex}\varphi} + U_L} \tag{35}$$

A more detailed analysis would consider the variation in the overall turbocharger efficiency η_{TC} in Eq. (32) with the working conditions. It depends on the respective inlet corrected mass flow rates through both turbomachines and respectively on π_c and π_e, indicated by the respective performance maps [59], and [50], among others. Solving the system of simultaneous equations taking into account this dependency is a classical turbomachine matching problem that is out of the scope of this study. Outputs of this matching process would be the shaft turning speed and the size and type of both turbomachines, compressor and turbine. Although this paper does not include such details, it is evident that an optimum choice for this application would be one-stage radial types owing to the moderate $\dot{m}$ envisaged. In the range of $1.5 < \pi_c < 3$, this type of turbomachines show a wide area of efficiencies near the maximum. The present study assumes commercial values of such efficiencies, following guidelines in an ample selection of open literature, such as [64], as a classical text, [67], and [68], for turbochargers of the size adequate for internal combustion engines, [69], for a wider view of mixed flow radial turbines, and [70], for general efficiency correlations for turbomachines.

It is well-known that the reachable maximum efficiencies, at the design point, are higher when the size of the turbomachine is larger, characterized by $\dot{m}$, and more generally for the Reynolds number of its rotor tip speed at the design point Re^* using density and viscosity at the inlet section. [71], coincide with other authors to estimate the size effect of centrifugal compressors found in typical of turbochargers (axial inlet, radial outlet, no stator guide vanes) with formulae like Eq. (36), where $_{ref}$ indicates reference values. According to real data, the exponent seems to decrease with Re^* down to near 0 for $Re^* > 10^6$. Capata and Sciuba in their publications [72], and [73], offer some comparisons among the different correction variants.

$$\frac{1-\eta_{ctt}}{1-\eta_{ctt,ref}} = \left(\frac{Re^*}{Re^*_{ref}}\right)^{0.1\text{to}0.25} \tag{36}$$

For centripetal turbines of turbochargers (radial inlet, axial outlet mixed flow, no stator guide vanes) [74], assumes a similar form of size correction. Some recent optimization studies on small-scale turbines predict a higher efficiency than what is found in commercial turbochargers, indicating the possibility of future better performing Brayton cycles for solar applications [75].

For compressors, [70], estimated a maximum achievable total to static $_{ts}$ polytropic $_{p}$ efficiency of $\eta_{cpts} = 0.8$, very near the total to total isentropic efficiency η_{ctt} owing to the moderate π_c, the high efficiency range dealt with, and the low exit Mach numbers. In parallel, for turbines, the maximum achievable polytropic efficiency estimated by [70], is $\eta_{epts} = 0.9$, very near the isentropic efficiency η_{ett} for the same reasons.

In respect to η_m, at the nominal operating point of the turbocharger, there is not much difference in its values either for plain, ball, and foil bearings, or magnetic levitation. At low speeds, plain bearings dissipate more power than the other two alternatives. For that, they need a higher oil circulation than ball bearings, but the power consumed is minute compared with $\dot{Q}_u$. The above-described analysis on design point efficiencies support the values taken in this paper and characterizes them as conservative and representative for the smallest facility sizes, below an orientative value of 50 kW of heat power.

Another issue is the time profile of η_{TC}, π_c, and π_e along one day when $\dot{m}$, p, and$T$ change as a response to a variable $\dot{q}_s$, and the resulting production profile. Additional considerations on thermal inertia, thermal energy storage, control, and partial load managing would be required that are out of the scope of this study. The low $\dot{q}_s$ near sunrise and sunset or during cloudy intervals would result in a low $\dot{m}$ resulting in a low π_c for a single fixed geometry turbocharger. This implies low values of η_{TC} because of off-design operation. This could be avoided either or both with variable geometry of the turbocharger and/or dual in-parallel turbochargers, operating with a single one at low $\dot{m}$. Reheating is also an option.

3.3. Direct heating efficiency

Let us define η^*_{TSAH} as a figure of merit for TSAH, analogous to η^*_{SAH} that is defined in Section 2 for SAH, Eq. (24). It allows to evaluate the performances of TSAH as well as to compare the two systems under similar operating conditions. η^*_{TSAH}, Eq. (37), does include optical losses in $\dot{q}_s$ (as commented in Section 2). The detailed variation of η_{op} with sun position and collector orientation is out of the scope of this work. The receiver efficiency η_r, Eq. (14), can be evaluated under the same mass flow rate $\dot{m}_{\dot{W}=0}$ and $T_{in} = T_2$, referred to as $\eta_{r,TSAH}$ in Eq. (38).

$$\eta^*_{TSAH} = \frac{\dot{m}_{W=0}(c_{p,4} T_{4t} - c_{p,atm} T_{atm})}{SlP^2_{ex}\dot{q}_s}; \tag{37}$$

$$\eta_{r,TSAH} = \frac{\dot{m}_{\dot{W}=0} c_{p,m}}{SlP^2_{ex} U_L}\left[1 - \exp\left(-\frac{SlP^2_{ex} U_L}{\dot{m}_{W=0} c_{p,m}\left(1 + \frac{U_L P_{ex}}{h_a P}\right)}\right)\right]\left[1 - \frac{U_L (T_2 - T_{amb})}{\dot{q}_s}\right] \tag{38}$$

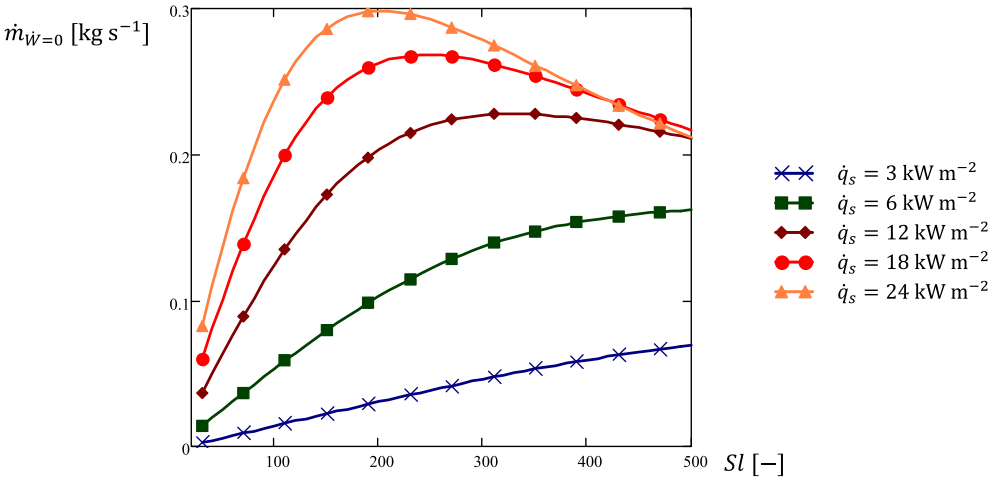

Fig. 7. TSAH mass flow rate at the freewheeling condition, $\dot{m}_{\dot{W}=0}$ versus Sl for several $\dot{q}_s$. $\pi_c = 2.5$, $\eta_{TC} = 0.51$, $\eta_{ett} = 0.75$, $\eta_{ctt} = 0.71$.

4. Results and TSAH assessment

The previous Section 3 develops a model for a global analysis of the TSAH concept. In the present section, the performances of the OAC variety of the Brayton cycle resulting from the TSAH concept are investigated under a variety of design parameters and working conditions to establish a framework for the development and application of the proposed technology. The language Mathcad® has been used for programming.

4.1. Concentrated irradiance and size

As stated in Section 3, considering constant values of η_{TC}, π_c and π_R, Eqs. (32) to (34) determine the mass flow rates $\dot{m}_{\dot{W}=0}$ corresponding to the freewheeling condition $\dot{W} = 0$. Fig. 7 shows the obtained results for Sl and $\dot{q}_s$ in the ranges of interest.

Once the mass flow rate for the freewheeling operation $\dot{m}_{\dot{W}=0}$ is established, Eq. (32), the corresponding T_{ou} results from solving Eq. (34). Solving Eq. (35) under $\dot{m}_{\dot{W}=0}$ results in $T_{w,ou}$ for any Sl and $\dot{q}_s$. Fig. 8 depicts $T_{w,ou}$ and the industry-standard thermal limit $T_{w,max}$.

In order to analyze the freewheeling condition, the results shown in Fig. 7 and Fig. 8 must be jointly considered, as they reveal the different effects of the design parameters on the operating condition of the whole system. Besides the receiver thermal losses, for any value ofSl and $\dot{q}_s$ the effects of Δp_{nrt} and T_{ou} are coupled to determine the freewheeling condition through $\dot{m}$. Considering a given $\dot{q}_s$, the influence of Sl on$\dot{m}_{\dot{W}=0}$, T_{ou} and $T_{w,ou}$ can be explained as follows:

- Due to the available solar power and the corresponding $\dot{Q}_u$,low Sl collectors operate with a small mass flow rate to reach enough temperature T_{ou} to provide the needed mechanical power through the turbine, Eq. (32) and Eq. (34).
- On the other hand, a low $\dot{m}$ induces a small pressure drop Δp_{nrt}, Eq. (33), which is beneficial for the freewheeling condition, allowing a moderate T_{ou}, as it results from Eq. (32).
- From that condition, increasing Sl results in a higher Δp_{nrt}, Eq. (33), which reduces the available pressure at the turbine inlet, requiring higher T_{ou} to hold the freewheeling condition, as Eq. (32) states. Fig. 8 shows the growing trend of T_{ou} with Sl.
- The influence of Sl on $\dot{m}_{\dot{W}=0}$, and $T_{w,ou}$ changes from low Sl to high Sl regions. Due to the low $\dot{m}$, small collectors with low Sl work with low heat transfer coefficient h_a and the associated high wall over temperature ΔT_w, which results in high thermal losses to ambient and the consequent low $\eta_{r,TSAH}$as well as high $T_{w,ou}$. Augmenting $\dot{m}_{\dot{W}=0}$ has a beneficial effect on $\eta_{r,TSAH}$ increasing the available $\dot{Q}_u$ limiting T_{ou}, Eq. (32). For relatively low $\dot{m}_{\dot{W}=0}$, the increase of Δp_{nrt} with this parameter is not the predominant factor in Eq. (32). A larger $\dot{m}_{\dot{W}=0}$can be noted in Fig. 7 while a remarkable $T_{w,ou}$ drop for larger Sl can be observed in Fig. 8 in the low Sl region. Conversely, the effect of mass flow rate on Δp_{nrt} hence on freewheeling is predominant for the large Sl region. Moreover, the beneficial contribution of $\dot{m}_{\dot{W}=0}$ on thermal losses disappears, since $T_{w,ou}$ grows following T_{ou},although $\Delta T_{w,ou}$ diminishes, as Fig. 8 shows. As a result, $\dot{m}_{\dot{W}=0}$ drops with large Sl, Fig. 7, while $T_{w,ou}$ and T_{ou} increase. This dependence on Sl is valid for any value of $\dot{q}_s$, although it is flatter for low $\dot{q}_s$ while it is sensitive for larger $\dot{q}_s$ due to higher mass flow rates and $\Delta T_{w,ou}$ involved.

Fig. 8 shows that under the freewheeling condition, for both very small and high Sl, $T_{w,ou} > T_{w,max}$, when operating with either medium or high $\dot{q}_s$ for the considered range of values. The increase in $\dot{q}_s$ reduces to a small range the values of Sl that allow $T_{w,ou} < T_{w,max}$. For any Sl, the value of $T_{w,ou}$ increases with $\dot{q}_s$ until it reaches a maximum allowed $\dot{q}_{s,max}$ corresponding to $T_{w,ou} = T_{w,max}$. Solving Eqs. (32) to (35) for $\dot{q}_s$ while assuming $T_{w,ou} = T_{w,max}$, provides the maximum allowed concentrated irradiance, $\dot{q}_{s,max}$, for any Sl, under the freewheeling condition, Eq. (39).

$$\dot{q}_{s,max} = \frac{h_a \langle \dot{m}_{\dot{W}=0} \rangle (T_{w,max} - T_{ou}) D}{D_{ex}} + U_L (T_{w,max} - T_{amb}) \tag{39}$$

Fig. 9 depicts the variation of the receiver tube efficiency from low to high Sls, obtained applying Eq. (38), as well as the relative total pressure drop evolution $\Delta p_{nrt}/p_{2t}$, Eq. (33), coherently with the previous analysis.

4.1.1. Maximum concentrated irradiance

Fig. 10 depicts $\dot{q}_{s,max}$ versus Sl under the freewheeling condition for constant $\pi_c = 2.5$ and $\eta_{TC} = 0.51$ as a reference case used also in the previous analysis. High concentrated irradiances are allowed for intermediates Sl while it is limited for either small or high Sl. Also, the influence of π_c and η_{TC} on the operating condition can also be observed in Fig. 10 where several $\dot{q}_{s,max}$ curves are reported for π_c = 2to3 and $\eta_{TC} = 0.47$ to 0.55.The consequence of increasing π_c can be explained on the fact that π_c involves two opposing effects: on the one hand, a higher π_c results in a higher $T_{in} = T_2$, Eq. (27), for the same $\Delta T = T_{ou} - T_{in}$ it leads to higher T_{ou}, thus higher $T_{w,ou}$, meeting thermal limits at lower $\dot{q}_s$. On the other hand, having a higher π_c has a beneficial effect reducing the pumping power thus decreasing the required T_{ou}

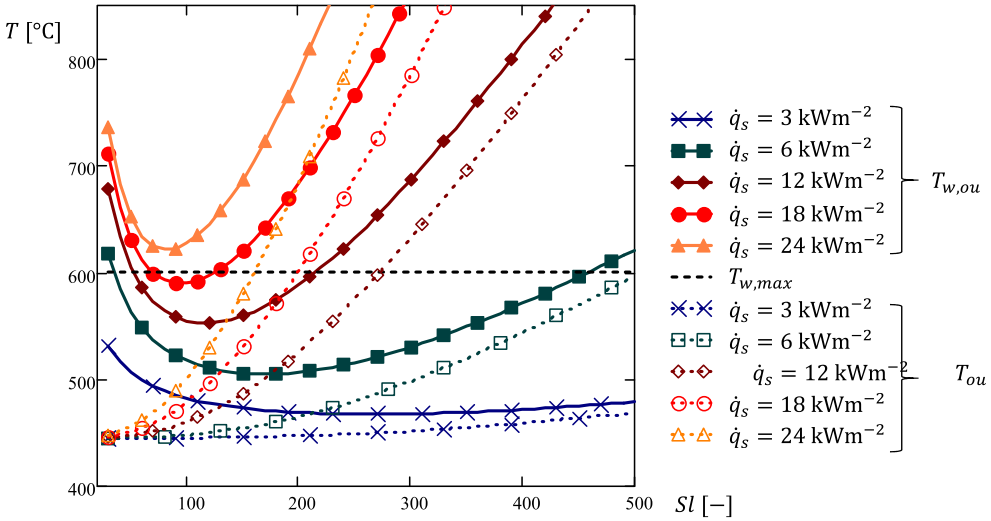

Fig. 8. TSAH wall temperature versusSl for several $\dot{q}_s$ under the freewheeling condition $\dot{W} = 0$. $\pi_c = 2.5$, $\eta_{TC} = 0.51$, $\eta_{ett} = 0.75$, $\eta_{ctt} = 0.71$, $T_{w,max} = 600$ °C.

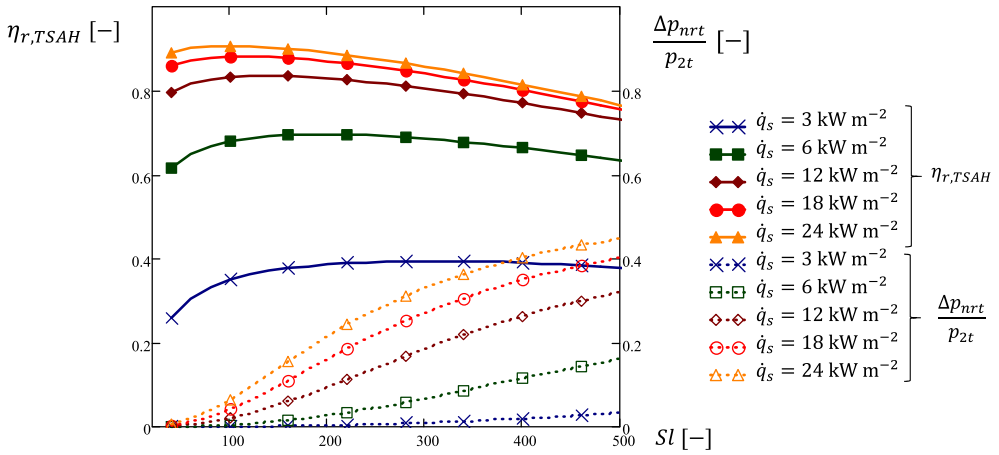

Fig. 9. TSAH receiver thermal efficiency$\eta_{r,TSAH}$ and relative total pressure drop $\Delta p_{nrt}/p_{2t}$ versusSl for several $\dot{q}_s$, corresponding to the freewheeling condition $\dot{m}_{W=0}$. $T_{amb} = T_{atm} = 10$ °C, $\pi_c = 2.5$, $\eta_{TC} = 0.51$, $\eta_{ett} = 0.75$, $\eta_{ctt} = 0.71$, $T_{w,max} = 600$ °C.

under the freewheeling condition. The results of $\dot{q}_{s,max}$ are either favorable or unfavorable depending on the combination of these two effects with the other operating parameters, as Fig. 10 indicates. The effect of varying π_c is further explained below, Fig. 15. An increase in the turbocharger global efficiency η_{TC} strongly affects the maximum acceptable concentrated irradiance, reducing the power needed from the turbine. Consequently, for a given $\dot{q}_s$ and Sl it allows reaching the freewheeling condition at lower T_{ou} and $T_{w,ou}$, increasing the operating mass flow rates and reaching the thermal limit at higher $\dot{q}_s$.

As a result of the present analysis, high concentration ratio C solar collectors are viable leading to about $100 < Sl < 500$ meaning high $\dot{q}_{s,max}$ for a given G_{bT}. This region is called from now on "critical". Smaller C are possible for larger Sl, meaning this a longer row installation with a fixed D_{ex}. Moreover, the desired mass flow rate can be split in a layout of parallel rows so that Sl can be positioned near the critical value.

All this indicates the feasibility of the design in a wide range of collector field aspect ratios and sizes. Considering the layout in Fig. 6, an upgrade for larger medium-scale installation would be replacing the supply tube, n with an even number of collector rows of the same length L_c, to approach a U-configuration. This reduces Δp_{fnt} allowing a slightly higher$\dot{q}_{s,max}$, besides eliminating the cost and losses of supply tubes, although the pressure loss of the T junctions must be added. They are needed, upstream the collector, to separate the flow for each row, and downstream it, to join the flows.

4.2. TSAH and SAH comparison

The efficiency parameter η^*_{TSAH}, already defined in Section 3, reveals additional information, as well as allowing a comparison with the SAH concept presented in Section 2, and depicted in Fig. 1. In order to compare the performances of the two considered systems, the SAH is set to produce hot air at the same delivery temperature $T_d = T_4$. That condition is matched when the proper mass flow rate is used, $\dot{m}_{SAH}$, which can be determined by rewriting Eq. (16) for $T_{out} = T_{dt}$ and $T_{in} = T_{atm} + \frac{W_p}{\dot{m}_{SAH} c_{p,p}} - \frac{v_{in}^2}{2c_{p,in}}$ as in Eq. (40).

$$\frac{\dot{q}_s c_{p,m}}{U_L}\left[1 - \exp\left(-\frac{SlP_{ex}^2 U_L}{\dot{m}_{SAH} c_{p,m}\left(1 + \frac{U_L P_{ex}}{h_a P}\right)}\right)\right]\left(1 - \frac{U_L(T_{in} - T_{amb})}{\dot{q}_s}\right) = (c_{p,d} T_{dt} - c_{p,int} T_{int}) \tag{40}$$

The SAH global efficiency η^*_{SAH}, receiver efficiency $\eta_{r,SAH}$, and pumping ratio $R_{p,SAH}$ are evaluated using Eqs. (25) and (22) with $\dot{m}_{Tou} = \dot{m}_{SAH}$, $T_{ou} = T_d = T_4$and T_{in}. For TSAH, the pumping ratio $R_{p,TSAH}$

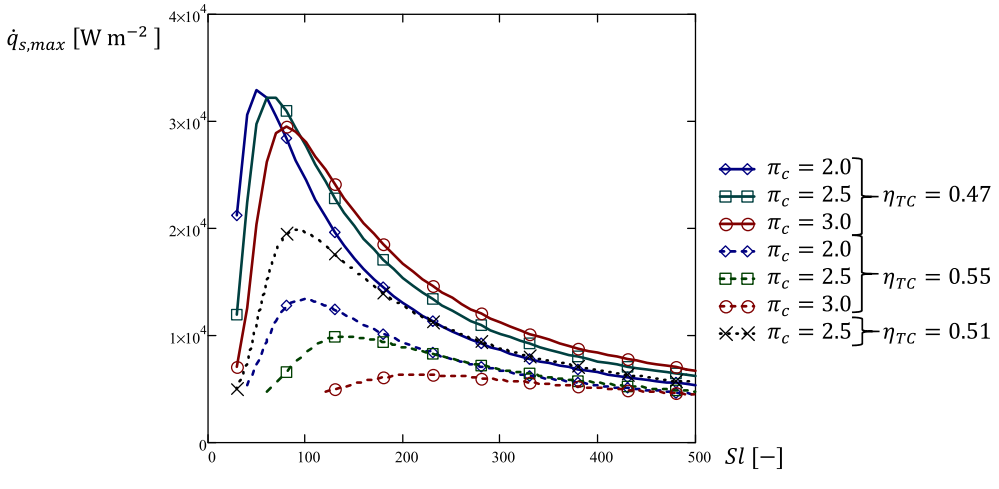

Fig. 10. TSAH allowed $\dot{q}_{s,max}$ under freewheeling condition $\dot{W} = 0$, versus Sl, for $\pi_c = 2$, 2.5, and3, for three efficiency cases: 1) low efficiency $\eta_{TC} = 0.47$, $\eta_{ett} = 0.72$, and $\eta_{ctt} = 0.69$ with dashed lines, 2) high efficiency $\eta_{TC} = 0.55$, $\eta_{ett} = 0.78$, $\eta_{ctt} = 0.74$ with continuous lines, and 3) intermediate $\eta_{TC} = 0.51$, $\eta_{ett} = 0.75$, $\eta_{ctt} = 0.71$, $\eta_m = 0.95$ with dot line.

can be evaluated using Eq. (33) with the incompressible approximation, as of being $\Delta p_{nrt}/p_{2t} < 1.0$, resulting in Eq. (41).

$$R_{p,TSAH} \approx \frac{\Delta p_{nrt}\dot{m}_{TSAH}}{\rho_m \dot{Q}_u} = \frac{\Delta p_{nrt} R_g (T_2 + T_3)/2}{p_2 \pi_c (c_{p,3} T_{3t} - c_{p,2} T_{2t})} \quad (41)$$

Fig. 11 depicts $\eta_{r,TSAH}$, η^*_{TSAH}, and $R_{p,TSAH}$evaluated under the freewheeling condition, thus with $\dot{m}_{\dot{W}=0}$, and maximum concentrated irradiance $\dot{q}_s = \dot{q}_{s,max}$, for any *Sl*. The same Fig. 11 shows the performances of SAH, in terms of $\eta_{r,SAH}$, η^*_{SAH}, and $R_{p,SAH}$ for the same delivery temperature $T_d = T_4$ and $\dot{q}_s = \dot{q}_{s,max}$. Mass flow rates $\dot{m}_{TSAH}$ and $\dot{m}_{SAH}$ are shown on the secondary axis. The figure also shows the air temperature at the TSAH turbine outlet, thus the delivery temperature to the user $T_d = T_4$ in non-dimensional form.

As previously mentioned, $\eta_{r,TSAH}$ increases for higher $\dot{q}_s$, so that in Fig. 11 it follows the same trend as$\dot{q}_{s,max}$, shown in Fig. 10. High *Sl* with low $\dot{q}_{s,max}$leads to lower $\eta_{r,TSAH}$. η^*_{TSAH} is slightly lower than $\eta_{r,TSAH}$. T_d varies slightly with *Sl*, remaining in the desired range of interest for industrial application T_d 350 to 450 °C. A SAH system operating with the same delivery temperature and $\dot{q}_s = \dot{q}_{s,max}$, shows a higher receiver efficiency $\eta_{r,SAH}$ due to lower mean wall temperature, hence lower thermal losses when compared to TSAH. However, η^*_{SAH} results to be much smaller, as it takes into account the primary energy consumption for pumping. This happens at high $\dot{q}_{s,max}$, typically in the intermediate *Sl* region. In fact, under these conditions, for $100 < Sl < 350$ TSAH offers higher performances than SAH, thus $\eta^*_{TSAH} > \eta^*_{SAH}$. At very large *Sl* and low $\dot{q}_{s,max}$, Fig. 10, $\eta^*_{TSAH} < \eta^*_{SAH}$ due to the strong drop of $\eta_{r,TSAH}$. Mass flow rates are slightly different, being $\dot{m}_{TSAH} < \dot{m}_{SAH}$, given that part of the energy is lost at the shaft of the turbo-compressor. The capability of TSAH to reduce the pumping power requirements, thus R_p, for similar mass flow rates, due to the higher density can be observed, as $R_{p,TSAH} < R_{p,SAH}$.

4.3. Reference case analysis

The maximum concentrated irradiance, as shown in Fig. 10, defines an upper limit of the range of $\dot{q}_s$ and *Sl*, corresponding to collector sizes, in which the system can operate, depending on several design parameters, η_{TC}, π_c, $T_{w,max}$, and *D*. Moreover, within this range, the performance of the system can vary remarkably. Considering a certain *Sl*, some further analysis reveals additional data for scrutinizing TSAH. Fig. 12 shows the temperature and the pressure at the relevant points of the cycle, according to Fig. 6, versus a range of $\dot{q}_s \le \dot{q}_{s,max}$, for a given turbocharger efficiencyη_{TC} and $\dot{W} = 0$.

A delivery temperature $T_d > 327$ °C is obtained at the turbine outlet as the main goal of the TSAH concept, without any external mechanical or electrical energy consumption. The delivery temperature $T_4 = T_d$ as well as T_2 and T_3 show a smooth profile versus$\dot{q}_s$, which indicates excellent stability under the typical variable working conditions of solar energy applications. T_d changes only 100 °C for a $\dot{q}_s$ range from 2.6 kW m^{-2} to 13.2 kW m^{-2}. In Fig. 12, one can observe that π_c has been kept constant, so that T_2 is also almost constant. $T_3 = T_{ou}$(according to Fig. 2) grows with $\dot{q}_s$ to increase the turbine power needed to compensate for the increased $\Delta p_{nrt} = p_{2t} - p_{3t}$, which results from a higher mass flow rate. $T_{w,ou}$ increases with $\dot{q}_s$ reaching $T_{w,ou} = T_{w,max}$ for $\dot{q}_s = \dot{q}_{s,max}$. Fig. 13 shows the mass flow rate versus $\dot{q}_s$. In the same figure, $\eta_{r,TSAH}$ evaluated at the same working condition, increases with $\dot{q}_s$ reaching its maximum value at $\dot{q}_s = \dot{q}_{s,max}$. Although the average wall temperature $T_{w,m}$ increases with $\dot{q}_{s,max}$ following $T_{w,ou}$, the ratio $U_L(T_{w,m} - T_{amb})/\dot{q}_s$ decreases, leading to higher thermal efficiency. η^*_{TSAH} follows the same trend, Fig. 13.

4.3.1. Delivery overpressure

The condition $T_{w,ou} \le T_{w,max}$ suggests the possibility of operating at higher temperatures T_{ou} and $T_{w,ou}$than the ones reported in Fig. 12, which have been evaluated using Eq. (32) with $\pi_R = 1$.Solving Eq. (32) for $\pi_R > 1$ means increasing the delivery pressure $p_d = p_{4t} = \pi_R p_{amb}$.

Delivering hot air with an over-pressure $\pi_R > 1$ can be of profit to the user process as a secondary mechanical power output of the TSAH concept. This means increasing the delivery pressure $p_d = p_{4t} = \pi_R p_{atm}$. Having $p_d > p_{atm}$ reduces the power extracted by the turbine, so that a higher $T_{ou} = T_3$ is needed to compensate for this power drop in order to keep the freewheeling condition. Solving Eq. (22) for $\pi_R > 1$ would result in higherT_{ou} than the ones shown in Fig. 12, which have been obtained for the reference case of $\pi_R = 1$. As seen in Fig. 12, for $\dot{q}_s < \dot{q}_{s,max}$ the wall temperature is below the thermal limit $T_{w,max}$. Although it is not possible to further increase T_{ou} for $\dot{q}_s = \dot{q}_{s,max}$ where $T_{w,ou} = T_{w,max}$, for $\dot{q}_s < \dot{q}_{s,max}$ higher T_{ou} and $T_{w,ou}$ can be permitted. Combining Eq. (32) with Eq. (7), the pressure ratio π_R corresponding to maximum wall temperature $T_{w,ou} = T_{w,max}$ can be found for any $\dot{q}_s$, π_c, and η_{TC} under the freewheeling condition, $\dot{m}_{W=0}$, Eq. (42).

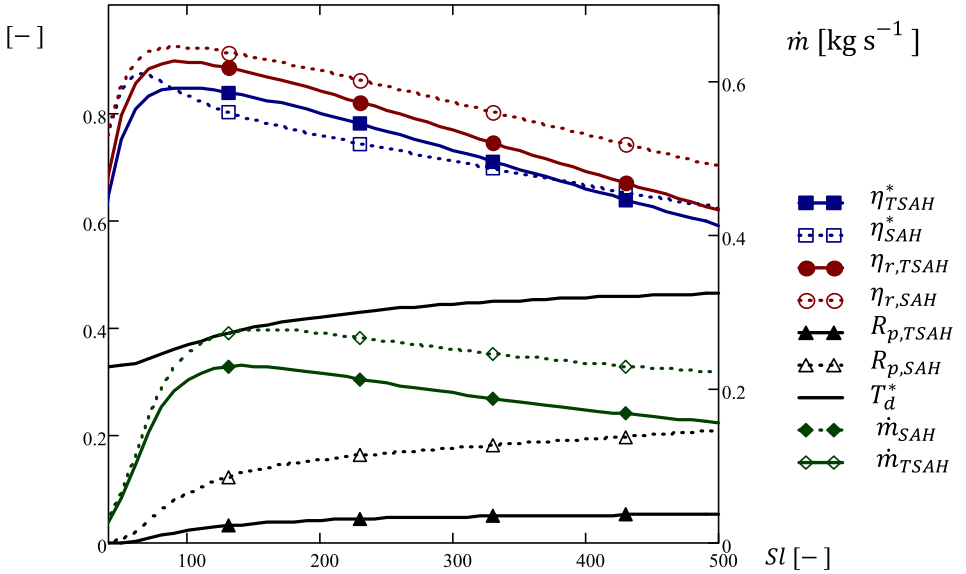

Fig. 11. Performances at $\dot{q}_{s,max}$ versus *Sl* under the freewheeling condition $\dot{W} = 0$. TSAH (solid lines) and comparison with SAH (dashed lines) producing air at the same outlet temperature. $\pi_c = 2.5$, $\eta_{TC} = 0.51$, $\eta_{ett} = 0.75$, $\eta_{ctt} = 0.71$, $T^*_d = T_4/1,000$ °C. Left axis for non-dimensional parameters.

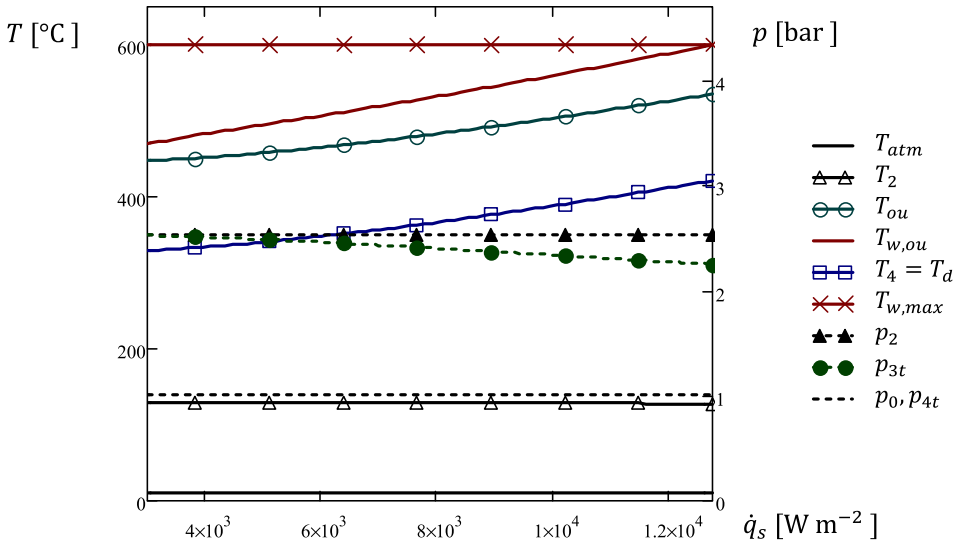

Fig. 12. Temperatures and pressures versus concentrated solar irradiance $\dot{q}_s$ for $Sl = 200$ under the freewheeling condition $\dot{W} = 0.\pi_c = 2.5$, $\eta_{TC} = 0.51$, $\eta_{ett} = 0.75$, $\eta_{ett} = 0.71$.

$$c_{p,c}T_{atm}\left(\pi_c^{\frac{\gamma_c-1}{\gamma_c}}-1\right)=\eta_{TC}c_{p,e}\left(T_{w,max}-\frac{D_{ex}(\dot{q}_s-U_L(T_{w,max}-T_{amb})}{h_a\langle\dot{m}_{\dot{W}=0}\rangle D\varphi}+\frac{v_3{}^2}{2c_{p,3}}\right)\left[1-\left(\frac{\pi_c(1-\frac{\Delta p_{nrt}\langle\dot{m}_{\dot{W}=0}\rangle}{p_{2t}})}{\pi_R}\right)^{-\frac{\gamma_e-1}{\gamma_e}}\right] \quad (42)$$

Fig. 14 shows the maximum allowed over-pressure ratio π_R evaluated for a given $Sl = 200$, and $\pi_c = 2.5$, for several η_{TC} in a wide range of $\dot{q}_s$,either for $\dot{q}_s < \dot{q}_{s,max}$ and $\dot{q}_s > \dot{q}_{s,max}$.

Coherently with the previous analysis, $\pi_R = 1$ for $\dot{q}_s = \dot{q}_{s,max}$, over-pressure ratios $\pi_R > 1$ are possible for $\dot{q}_s < \dot{q}_{s,max}$ as expected, confirming the possibility of delivering hot air at $p_d > p_{atm}$ under appropriate conditions. $\pi_R < 1$ is not physically possible because $p_d < p_{atm}$. Moreover, $\pi_R < 1$ approximately indicates the inverse of the over pressure that the auxiliary compressor must provide at the inlet section, point 1 in Fig. 6, to fulfill, Eq. (32).

The influence of the turbocharger efficiency η_{TC} on the performances is profound. In the case depicted in Fig. 14, a moderate increase, within what is possible with turbocharger technology, translates into a substantially higher $\dot{q}_{s,max}$, corresponding to $\pi_R = 1$. Moreover, at high values of η_{TC}, a substantial gain of over-pressure can be obtained for $\dot{q}_s < \dot{q}_{s,max}$.

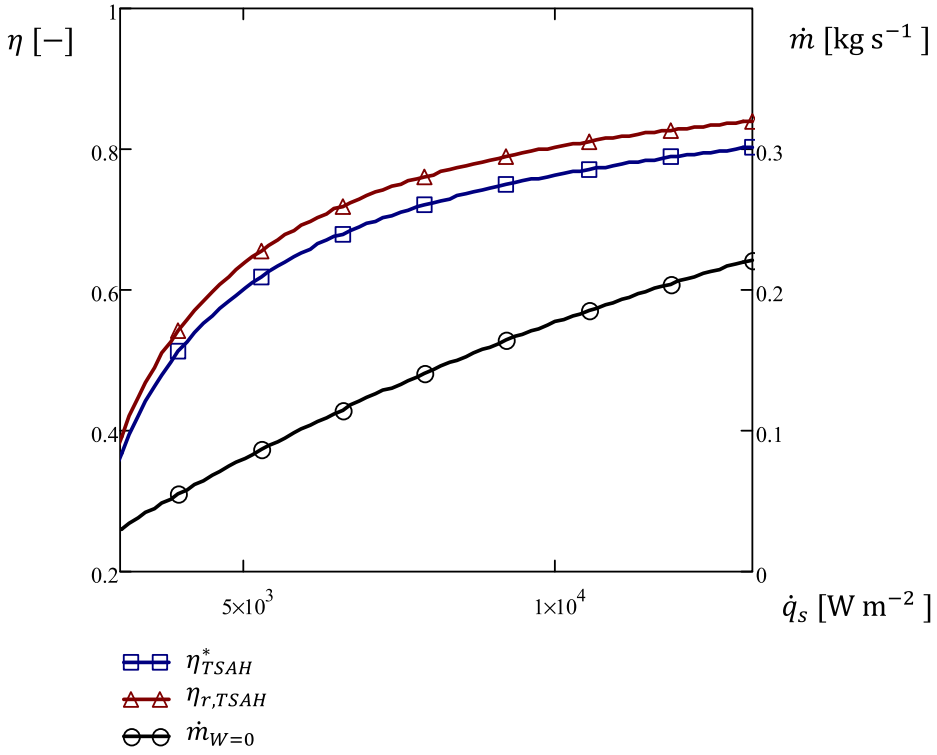

Fig. 13. Efficiency and mass flow rate versus concentrated solar irradiance $\dot{q}_s$ for $Sl = 200$, under the freewheeling condition $\dot{W} = 0.\pi_c = 2.5$, $\eta_{TC} = 0.51$, $\eta_{ett} = 0.75$, $\eta_{ett} = 0.71$.

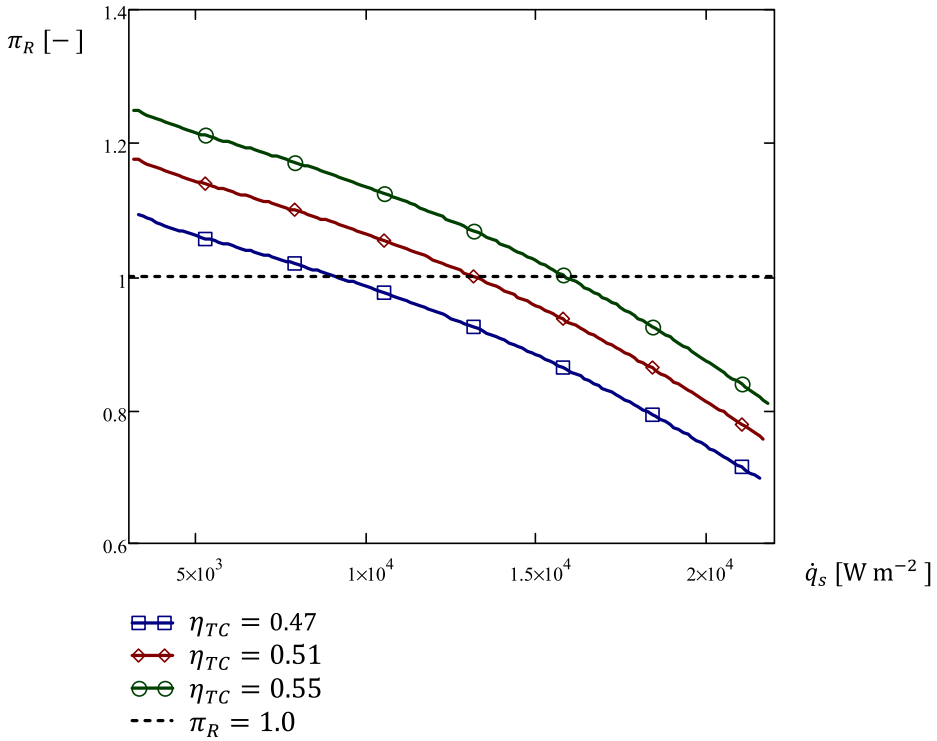

Fig. 14. Over-pressure ratio π_R versus concentrated solar irradiance $\dot{q}_s$ for η_{TC} = 0.47, 0.51, and0.55, under the freewheeling condition $\dot{W} = 0$. $Sl = 200$, $\pi_c = 2.5$, $T_{w,max} = 600$ °C.

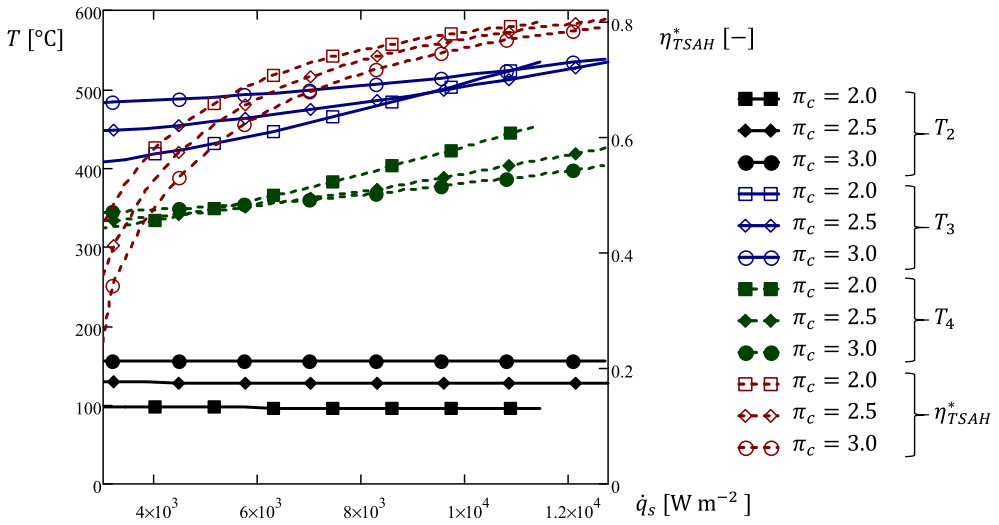

Fig. 15. TSAH main temperatures and efficiency versus concentrated solar irradiance $\dot{q}_s$ for several π_c, under the freewheeling condition $\dot{W} = 0$. $Sl = 200$, $\pi_R = 1.0$, $T_{w,max} = 600$ °C.

4.3.2. Compression ratio

Fig. 9 shows the influence of $\pi_c$on the operative condition of the TSAH concept, showing the variation of $\dot{q}_{s,max}$ with $\pi_c = 2.0$ to 3.0. Additional consideration on the role of π_c can be formulated analyzing Fig. 15, which shows the main operative temperatures as well as the TSAH efficiency η^*_{TSAH} versus $\dot{q}_s$, for several $\pi_c = 2.0$ to 3.0 for a reference collector with $Sl = 200$ versus $\dot{q}_s < \dot{q}_{s,max}$. The inlet receiver temperature T_2 is directly affected by π_c. Under the same $\dot{q}_s$, higher T_2 translates into a higher receiver outlet temperature $T_3 = T_{ou}$which is appreciable at low $\dot{q}_s$. For higher $\dot{q}_s$ the variation of T_3 is not appreciable. In fact, a higher π_c reduces the total pressure drop Δp_{nrt} due to the density increase, which is beneficial for the freewheeling condition, reaching it at lower T_{ou} and higher mass flow rates. The TSAH efficiency η^*_{TSAH} decreases slightly with π_c because of a higher average temperature $T_m = (T_2 + T_3)/2$. Delivery temperature T_d increases with π_c, being π_e π_c and $T_d = T_4$. In general terms, the effect of varying π_c in the range 2–3 seems not affecting remarkably the TSAH behavior, highlighting its excellent flexibility concerning this parameter.

4.4. TSAH assessment highlights

The analysis carried out in this section establishes the framework of the application of the TSAH concept presented in Section 3. The freewheeling condition for the turbocharger to operate without any additional external power input has been verified over a wide range of collector layouts. The high-temperature limit established according to the receiver tube requirements defines the maximum allowable

concentrated irradiance $\dot{q}_s$for any non-dimensional length Sl. As a result, collectors with intermediate Sl 100to350 can operate at high $\dot{q}_s$, corresponding to larger collector aperture widths for a nominal irradiance. Within this range, TSAH can reach the highest efficiency η^*_{TSAH} since it increases with $\dot{q}_s$. Although with lower efficiency, a TSAH can be implemented using smaller aperture widths up to $Sl = 500$, either using PTC or LFC types, demonstrating excellent design flexibility. The turbocharger efficiency η_{TC} is of significant influence to boost the TSAH performances. Besides an overall efficiency reduction, a TSAH operating at $\dot{q}_s < \dot{q}_{s,max}$ provides air at 330 °C $< T_d <$ 430 °C within the searched thermal level. A moderate air delivery over-pressure is possible for $\dot{q}_s < \dot{q}_{s,max}$, as secondary valuable output to the user. The pressure ratio has not a remarkable effect on TSAH operation when varying within a reasonable range $\pi_c = 2$ to 3.

Comparing TSAH with the simpler SAH working with the same delivery temperature and$\dot{q}_s$,TSAH shows better performances being $\eta^*_{TSAH} > \eta^*_{SAH}$ in the range of Sl 100 to 350. Besides efficiency comparison, TSAH is preferable to SAH since it does not require any additional pumping power consumption, pointing out to lower operating costs, besides to be a wholly renewable and greenhouse gases-free application.

5. Conclusions and further work

The present study identifies and highlights the importance of decarbonizing and greening industrial processes that consume heat following institutional recommendations and recent researches. More particularly, it underpins those consuming hot air. Directly heating atmospheric air to medium temperatures inside linear concentrating solar collectors, such as LFC and PTC types, has not been a common practice, although simpler, cheaper, and lighter solar facilities are possible avoiding liquid HTFs, at the same time avoiding dangerous leakages and expenses for its replacement.

The viability analysis performed in this study assures the technical feasibility of direct air heating with conventional medium-temperature solar concentrating collectors, providing the design parameters and figures of merit for optimizing the performances of the proposed concepts. The main findings are as follows:

- The direct heating of ambient air at atmospheric pressure OAC-SAH is viable with conventional medium-temperature solar collectors using standard evacuated tubes manufactured for solar thermal power plants. The air can be supplied to the user in the range of 300–450 °C with specific collector layouts characterized by the here introduced tube slenderness parameter Sl. This procedure requires external pumping power, with a large consumption for long rows of collectors, which can appear in large-scale facilities, as they would be characterized by $Sl \gg 1$ when using industry-standard receiver tubes. Rearranging the facility with a smaller Sl can reduce this consumption; but still, pumping air needs some power.
- The direct air heating boosted by a turbocharger TSAH allows supplying the user with hot air up to 400 °C canceling the need for external pumping power under suitable working conditions, which can be achieved in a wide range of collector sizes. For the turbocharger efficiency to be high enough, the TSAH concept can supply the user process with hot air at a slight pressure over atmospheric for coping with the process pressure losses. The results reveal the existence of an optimal range for the non-dimensional tube slenderness $Sl = L/P_{ex}$. It indicates the optimum aspect ratio of the solar field collector rows of length L when it is combined with the concentrated solar irradiance $\dot{q}_s$ captured by the receiver tube external perimeter P_{ex} as a result of the optical concentration and efficiency of the collector. High compressor and turbine efficiencies are of paramount importance, as in any Brayton cycle, as well as limiting the pressure losses, not only on the receiver tubes but also on the supply and return circuits.
- Receiver tube diameters larger than conventional, eventually incorporating internal fins, would be beneficial for both the SAH and TSAH concepts, although the proposed TSAH concept is valid with the usual 70 mm O. D. commercial evacuated tubes.

The positive results recommend further theoretical studies to characterize the partial load operation, production profiles, full costs breakdown, and either the convenience of heat storage or a complementary source of reheating to fill solar gaps. In a further stage, pilot plant experimental validations seem highly necessary as well as a joint technological development toward enabling industrial agents to offer the users reliable products for evolving to a cleaner and less carbon-intensive industrial processes.

Declaration of Competing Interest

The authors declare that they have no known competing financial interests or personal relationships that could have appeared to influence the work reported in this paper.

Acknowledgments

This research was supported by the Industrial Ph.D. program of Comunidad de Madrid, Spain (BOCM Reference IND2017/AMB7769).

Appendix A. Supplementary material

Supplementary data to this article can be found online at https://doi.org/10.1016/j.applthermaleng.2020.114914.

References

[1] U.S. Energy Information Administration, INTERNATIONAL ENERGY OUTLOOK 2018, 24 07 2018. [Online]. Available: https://www.eia.gov/outlooks/ieo/. [Accessed 13 10 2018].
[2] International Energy Agency, World Energy Outlook 2017, International Energy Agency, Paris, 2017.
[3] British Petroleum, BP Energy Outlook. 2017 Edition, British Petroleum, London, 2017.
[4] F. Princiotta, D.H. Loughlin, Global climate change: The quantifiable sustainability challenge, J. Air Waste Manag. Assoc. 64 (9) (2014) 979–994.
[5] International Energy Agency, IEA Solar Heating & Cooling Programme, 13 10 2018. [Online]. Available: https://www.iea-shc.org/.
[6] R. Wang, Z. Xu, T. Ge, Introduction to solar heating and cooling systems, Advances in Solar Heating and Cooling, Woodhead Publishing, 2017, pp. 3–12.
[7] T. Razykov, C. Ferekides, D. Morel, E. Stefanakos, H. Ullal, H. Upadhyaya, Solar photovoltaic electricity: Current status and future prospects, Sol. Energy 85 (8) (2011) 1580–1608.
[8] M. Patel, Wind and Solar Power Systems, CRC Press, Boca Raton, 2006.
[9] European Commission, Heating and cooling, Brussels, 2018.
[10] Solar Heat Europe, Solar Heat Europe, 13 10 2018. [Online]. Available: http://solarheateurope.eu/.
[11] The European Technology Platform on Renewable Heating and Cooling, Solar Heating and Cooling. Technology Roadmap, Brussels, 2014.
[12] European Commission, An EU Strategy on Heating and Cooling, Brussels, 2016.
[13] S. Farjana, N. Huda, M. Parvez Mahmud, R. Saidur, Solar process heat in industrial systems – A global review, Renew. Sustain. Energy Rev. 82 (3) (2018) 2270–2286.
[14] S. Kalogirou, The potential of solar industrial process heat applications, Appl. Energy 76 (4) (2006) 337–361.
[15] IRENA, Solar heat for industrial processes - Technology Brief. IEA-ETSAP and IRENA Technology Brief E21, International Renewable Energy Agency, 2015.
[16] S. Mekhilef, V. Saidur, A. Safari, A review on solar energy use in industries, Renew. Sustain. Energy Rev. 15 (4) (2011) 1777–1790.
[17] ESTIF, Solar heating and Cooling Technology Roadmap, European Solar Thermal Industry Federation, European Technology Platform on Renewable Heating and Cooling, 2014.
[18] CTAER-SOLARCONCENTRA, MERCADO POTENCIAL EN ESPAÑA Y APLICACIONES EN TECNOLOGÍAS SOLARES DE CONCENTRACIÓN DE MEDIA TEMPERATURA, Ministerio de Economía y Competitividad, Madrid, 2015.
[19] I. Lillo-Bravo, E. Pérez-Aparicio, N. Sancho-Caparrini, M. Silva-Pérez, Benefits of medium temperature solar concentration technologies as thermal energy source of industrial processes in Spain, Energies (2018) 2950–2980.
[20] A. Sharma, C. Sharma, S. Mullick, T. Kandpal, Solar industrial process heating: A review, Renew. Sustain. Energy Rev. 78 (2017) 124–137.
[21] A. Sharma, C. Chen, N. Lan, Solar-energy drying systems: A review, Renew. Sustain. Energy Rev. 13 (6–7) (2009) 1185–1210.

[22] I. Dincer, On energetic, exergetic and environmental aspects of drying systems, Int. J. Energy Res. 26 (8) (2001) 717–727.
[23] R. Bahu, Energy consumption in dryer design, Drying (1991) 553–557.
[24] G. Pirasteh, R. Saidur, S. Rahman, N. Rahim, A review on development of solar drying applications, Renew. Sustain. Energy Rev. 31 (2014) 133–148.
[25] V. Belessiotis, E. Delyannis, Solar drying, Sol. Energy 85 (8) (2011) 1665–1691.
[26] P. Lewicki, Design of hot air drying for better foods, Trends Food Sci. Technol. 17 (4) (2006) 153–163.
[27] C. Ratti, Hot air and freeze-drying of high-value foods: a review, J. Food Eng. 49 (4) (2001) 311–319.
[28] R.S.A. Tripathy, S. Sahoo, H. Bindra, Performance analysis of receiver of parabolic trough solar collector: Effect of selective coating, vacuum, and semitransparent glass cover, Int. J. Energy Res. 42 (2018) 4235–4249.
[29] R. Grena, P. Tarquini, Solar linear Fresnel collector using molten nitrates as heat transfer fluid, Energy 36 (2) (2011) 1048–1056.
[30] D. Pietruschka, R. Fedrizzi, F. Orioli, R. Söll, R. Stauss, Demonstration of three large scale solar process heat applications with different solar thermal collector technologies, Energy Procedia 30 (2012) 00.
[31] F. Xuening, C. Lei, D. Yuman, J. Min, F. Jinping, CFD modeling and analysis of brine spray evaporation system integrated with solar collector, Desalination 366 (2015) 139–145.
[32] A. Shukla, D. Nkwetta, Y. Cho, V. Stevenson, P. Jones, A state of art review on the performance of transpired solar collector, Renew. Sustain. Energy Rev. 16 (6) (2012) 3975–3985.
[33] A. Saxena, Varun, A. El-Sebaii, A thermodynamic review of solar air heaters, Renew. Sustain. Energy Rev. 43 (2015) 863–890.
[34] M. Kumar, S. Sansaniwal, P. Khatak, Progress in solar dryers for drying various commodities, Renew. Sustain. Energy Rev. 55 (2016) 346–360.
[35] P. Good, G. Ambrosetti, A. Pedretti, A. Steinfeld, A 1.2MWth solar parabolic trough system based on air as heat transfer fluid at 500°C — Engineering design, modelling, construction, and testing, Sol. Energy 139 (2016) 398–411.
[36] E. Bellos, C. Tzivanidis, K. Antonopoulos, A detailed working fluid investigation for solar parabolic trough collectors, Appl. Therm. Eng. 114 (2017) 374–386.
[37] F. Incropera, D. DeWitt, T. Bergman, A. Invine, Fundamentals of Heat and Mass Transfer, New York, John Wiley, New York, 2007.
[38] G. Zhu, T. Wendelin, M. Wagner, C. Kutscher, History, current state, and future of linear Fresnel concentrating solar collectors, Sol. Energy 103 (2014) 639–652.
[39] Archimede Solar Energy, Solar Receiver Tubes for Thermodynamic Power Plants, [Online]. Available: http://www.archimedesolarenergy.it/en_home.asp. [Accessed 14 10 2018].
[40] SCHOTT North America, Inc., The SCHOTT PTR®70 Receiver Platform, 2018. [Online]. Available: https://www.us.schott.com/csp/english/schott-solar-receivers.html.
[41] E. Bellos, C. Tzivanidis, I. Daniil, K.A. Antonopoulos, The impact of internal longitudinal fins in parabolic trough collectors operating with gases, Energy Convers. Manage. 135 (2017) 35–54.
[42] P. Good, G. Ambrosetti, A. Pedretti, A. Steinfeld, An array of coiled absorber tubes for solar trough concentrators operating with air at 600°C and above, Sol. Energy 111 (2015) 378–395.
[43] Y. Soo Too, R. Benito, Enhancing heat transfer in air tubular absorbers for concentrated solar thermal applications, Appl. Therm. Eng. 50 (1) (2013) 1076–1083.
[44] R. Bader, A. Pedretti, M. Barbato, A. Steinfeld, An air-based corrugated cavity-receiver for solar parabolic trough concentrators, Appl. Energy 138 (2015) 337–345.
[45] W. Fuqiang, C. Ziming, T. Jianyu, Y. Yuan, S. Yong, L. Linhua, Progress in concentrated solar power technology with parabolic trough collector system: A comprehensive review, Renew. Sustain. Energy Rev. (2017) 1314–1328.
[46] J. Muñoz-Anton, M. Biencinto, E. Zarza, L. Díez, Theoretical basis and experimental facility for parabolic trough collectors at high temperature using gas as heat transfer fluid, Appl. Energy 135 (2014) 373–381.
[47] M. Roldán, L. Valenzuela, E. Zarza, Thermal analysis of solar receiver pipes with superheated steam, Appl. Energy 103 (2013) 73–84.
[48] E. Bellos, C. Tzivanidis, Parametric investigation of supercritical carbon dioxide utilization in parabolic trough collectors, Appl. Therm. Eng. 127 (2017) 736–747.
[49] E. Bellos, C. Tzivanidis, K.A. Antonopoulos, I. Daniil, The use of gas working fluids in parabolic trough collectors – An energetic and exergetic analysis, Appl. Therm. Eng. 109 (2016) 1–14.
[50] D. Wilson, T. Korakianitis, The Design of High-efficiency Turbomachinery and Gas Turbines, 2nd ed., MIT Press, Cambridge, Massachusetts, 1998.
[51] E. Bellos, C. Tzivanidis, K.A. Antonopoulos, Parametric analysis and optimization of a solar assisted gas turbine, Energy Convers. Manage. 137 (2017) 151–165.
[52] A. Cinocca, R. Cipollone, R. Carapellucci, V. Iampieri, R. Mattia, CSP-PT gas plant using air as Heat Transfer Fluid with a packed bed storage section, Energy Procedia (2018).
[53] R. Forristal, Heat Transfer Analysis and Modeling of a Parabolic Trough in Engineering Equation Solver, US Department of Energy, Oak Ridge, 2003.
[54] F. Zaversky, R. Medina, J. García-Barberena, M. Sánchez, D. Astrain, Object-oriented modeling for the transient performance simulation of parabolic trough collectors using molten salt as heat transfer fluid, Sol. Energy 95 (2013) 192–215.
[55] J.A. Duffie, W.A. Beckman, Solar Engineering of Thermal Processes, Hoboken, John Wiley & Sons, New Jersey, 1991.
[56] H. Zellnik, S. Churchill, Convective heat transfer from High-Temperature air inside a tube, A.I. Ch.E. Journal 4 (1) (1958) 37–42.
[57] A. Lecuona-Neumann. Spain Patent P201630068, 21 1 2016.
[58] N. Watson, M. Janota, Turbocharging the Internal Combustion Engine, Palgrave, London, 1982.
[59] S. Dixon, Fluid Mechanics and Thermodynamics of Turbomachinery, fourth ed., Butterworth-Heinemann, 1978.
[60] H.a.A.R. Gaul, Incidence angle modifier and average optical efficiency of parabolic trough collectors, J. Sol. Energy Eng. 102 (1) (1980) 16–21.
[61] S. Karathanasis, Linear Fresnel Reflector Systems for Solar Radiation Concentration, Springer International Publishing, 2019.
[62] A. Lecuona, A. Famiglietti, M. Legrand, Theoretical study of direct vapor generation for energy integrated solar absorption machines, Renewable Energy 135 (May 2019) 1335–1353.
[63] S. Herrmann, H.J. Kretzschmar, V.E.V. Teske, P. Ulbig, R. Span, D.P. Gatley, Properties of humid air for calculating power cycles, J. Eng. Gas Turbines Power 132 (9) (2010) 093001.
[64] J. Heywood, Internal Combustion Engine Fundamentals, McGraw-Hill, New York, 1988.
[65] H. Saravanamuttoo, G.F.C. Rogers, H. Cohen, P. Straznicky, A. Nix, Gas Turbine Theory, Pearson, USA, 2017.
[66] B.S. Massey, Mechanics of Fluids, 8th ed., Taylor & Francis, 2006.
[67] J. El Hadef, G. Colin, V. Talon, Y. Chamaillard, New physics-based turbocharger data-maps extrapolation algorithms: validation on a spark-ignited engine, 2012 IFAC Workshop on Engine and Powertrain Control, Simulation and Modeling (ECOSM), Rueil-Malmaison, (2012).
[68] K. Stricker, L. Kocher, E. Koeberlein, D.G. Van Alstine, G.M. Shaver, Turbocharger map reduction for control-oriented modeling, J. Dyn. Sys. Meas. Control 136 (4) (2014) 0410081–0410081-14.
[69] S. Zhu, K. Deng, S. Liu, Modeling and extrapolating mass flow characteristics of a radial turbocharger turbine, Energy 87 (2015) 628–637.
[70] O. Balje, Turbomachines, John Wiley, New York, 1981.
[71] C. Weigel, C. Ball, Reynolds Number Effect on Overall Performance pf a 10.8 centimeter (4.25 inch) Sweptback Bladed Centrifugal Compressor, NASA, Cleveland, Ohio, 1972.
[72] R. Capata, E. Sciubba, Use of modified Balje maps in the design of low reynolds number turbocompressors, ASME IMECE 2012, Houston, (2012).
[73] R. Capata, E. Sciubba, Experimental fitting of the re-Scaled Balje maps for Low-Reynolds radial turbomachinery, Energies 8 (8) (2015) 7986–8000.
[74] E. Balje, A study on Reynolds number effects in turbomachines, J. Eng. Power 86 (3) (1964) 227.
[75] A.M. Daabo, A. Al Jubori, S. Mahmoud, R. Al-Dadah, Development of three-dimensional optimization of a small-scale radial turbine for solar powered Brayton cycle application, Appl. Thermal Eng. 111 (2017) 718–733.
[76] M. Lewis, Physical Properties of Foods and Food Processing Systems, Chichester, Ellis Horwood, UK, 1987.
[77] M. Sodha, et al., Solar Crop Drying, vol. 1, CRC Press, Boca Raton, Florida, USA, 1987.